Condensed Matter Physics 2010, Vol. 13, No 1, 13706: 1–26

http://www.icmp.lviv.ua/journal

CONDENSED MATTER PHYSICS

Thermodynamics, dielectric permittivity and phase diagrams of the $Rb_{1-x}(NH_4)_xH_2PO_4$ type proton glasses

S.I. Sorokov, R.R. Levitskii, A.S. Vdovych

Institute for Condensed Matter Physics of the National Academy of Sciences of Ukraine,
1 Svientsitskii Str., 79011 Lviv, Ukraine

Received January 18, 2010, in final form February 26, 2010

The cluster pseudospin model of proton glasses, which takes into account the energy levels of protons around the PO_4 group, the long-range interactions between the hydrogen bonds, and an internal random deformational field is used to investigate thermodynamical characteristics, longitudinal and transverse dielectric permittivities of $Rb_{1-x}(ND_4)_xD_2PO_4$ and $Rb_{1-x}(NH_4)_xH_2AsO_4$ compounds. A review of experimental and theoretical works on the $Rb_{1-x}(NH_4)_xH_2PO_4$ type crystals is presented.

Key words: *proton glass, dielectric permittivity*

PACS: *75.10.Nr, 77.22.Ch, 77.22.Ej, 77.22.Gm, 77.84.Fa*

1. Introduction. Literature review

1.1. Experimental studies of the $Rb_{1-x}(NH_4)_xH_2PO_4$ type compounds

The hydrogen bonded compounds of the $Rb_{1-x}(NH_4)_xH_2PO_4$ type, which at certain compositions have a proton glass phase, have been intensively studied for more than 25 years. In order to describe possible proton configurations in the mixed $Rb_{1-x}(NH_4)_xH_2PO_4$ type compounds, let us consider first the structure of the pure RDP-RbH_2PO_4 and ADP-$NH_4H_2PO_4$ crystals. In figure 1 a unit cell of the KDP-KH_2PO_4 crystal, which is isomorphic to RDP, is shown. A primitive cell

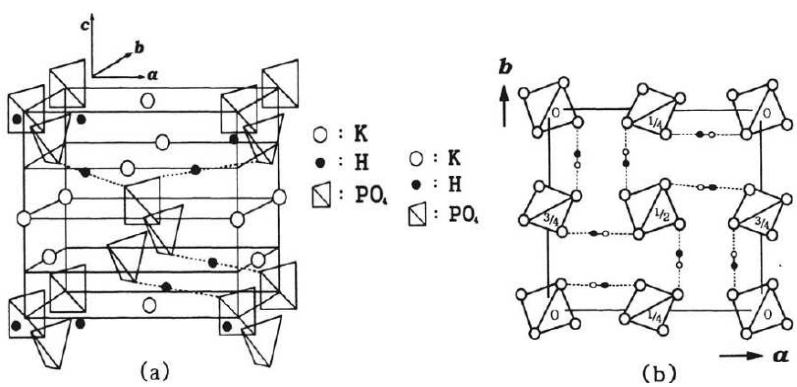

Figure 1. A unit cell (four formula units) of the KDP-KH_2PO_4 crystal.

of the RbH_2PO_4 type compounds contains one PO_4 tetrahedron of the "A" type and one PO_4 tetrahedron of the "B" type, two Rb atoms and four protons on four hydrogen bonds attached to the "A" type tetrahedron. In the ferroelectric phase the net dipole moment of the primitive cell, associated with displacements of heavy ions and deformations of the PO_4 groups, is directed along the c axis. A triggering mechanism of the ionic displacements in these crystals is the proton ordering (their positions are described by pseudospin operators $S_f = \pm 1,\ f = 1, 2, 3, 4$) in double

potential wells on the hydrogen bonds. The bond dipole moments lie almost in the ab plane; the total dipole moment of protons in the cell of the RDP type crystals is zero. Thus,

$$\vec{\mu}_{1\alpha} = (\mu^x_\alpha, 0, 0), \qquad \vec{\mu}_{3\alpha} = (-\mu^x_\alpha, 0, 0), \qquad \vec{\mu}_{2\alpha} = (0, -\mu^y_\alpha, 0), \qquad \vec{\mu}_{4\alpha} = (0, \mu^y_\alpha, 0),$$

where $\vec{\mu}_{f\alpha}$ are the dipole moments of the f-th hydrogen bond; $\alpha = +$ for $x = 0$, and $\alpha = -$ for $x = 1$.

The composition range in these compounds can be divided into three regions of x, which we shall call the glass phase region, the ferroelectric phase region, and the antiferroelectric phase region. The glass phase region exists in the $Rb_{1-x}(NH_4)_xH_2PO_4$ system at $x \sim 0.22 - 0.75$, in the $Rb_{1-x}(ND_4)_xD_2PO_4$ at $x \sim 0.23 - 0.65$, in the $Rb_{1-x}(NH_4)_xH_2AsO_4$ at $x \sim 0.2 - 0.45$, and in the $K_{1-x}(NH_4)_xH_2PO_4$ system at $x \sim 0.23 - 0.67$. The ferroelectric phase region lies between $x = 0$ and the glass phase region; the antiferroelectric phase region lies between $x = 1$ and the glass phase region. An important characteristic of the $Rb_{1-x}(NH_4)_xH_2PO_4$ type compounds is the Edwards-Anderson parameter $q_{\rm EA}$, which is the averaged over configurations square of the averaged over the Gibbs ensemble $S_{\rm f}$-operator. It is different from zero at $0 < x < 1$ at all temperatures; this will be shown hereinafter.

Glass phase composition region

In the proton glass phase there is no net spontaneous polarization, but the unit cell polarization is different from zero. This means that the average over the sample square of the cell dipole moment (proportional to the Edwards-Anderson parameter) is different from zero.

Experimental measurements of the dielectric permittivity of $Rb_{1-x}(NH_4)_xH_2PO_4$ [1–8], $Rb_{1-x}(ND_4)_xD_2PO_4$ [7, 9–14], $Rb_{1-x}(NH_4)_xH_2AsO_4$ [15–18], and $K_{1-x}(NH_4)_xH_2PO_4$ [19–23] in the glass phase composition region have shown that the temperature curves of the longitudinal $\varepsilon_{33}(T,\nu)$ and transverse $\varepsilon_{11}(T,\nu)$ permittivities are qualitatively similar. At high temperatures the real parts of the permittivities are roughly described by the Curie-Weiss law. Below a certain temperature $T_{\rm f}$, a deviation from the Curie-Weiss law is observed. Then $\varepsilon'_{33}(T,\nu)$ and $\varepsilon'_{11}(T,\nu)$ have maxima at temperature $T_{\rm m}$ and then slowly decrease. Below a certain temperature $T_{\rm g}$ (the inflection points) $\varepsilon'_{33}(T,\nu)$ and $\varepsilon'_{11}(T,\nu)$ rapidly fall to their minimal values. The imaginary parts of the permittivities $\varepsilon''_{33}(T,\nu)$ and $\varepsilon''_{11}(T,\nu)$ have peaks at $T_{\rm g}$ and fall nearly to zero at other temperatures. It should be noted that the temperatures $T_{\rm f}$, $T_{\rm m}$, and $T_{\rm g}(\nu)$ determined from $\varepsilon'_{33}(T,\nu)$ are somewhat different from those determined from $\varepsilon'_{11}(T,\nu)$.

The temperature $T_{\rm g}(\nu)$ decreases with decreasing frequency ν, at which the permittivity is measured. The temperature of the transition to the glass phase is T_0, where $T_{\rm g}(\nu) \to T_0$ at $\nu \to 0$. The character of the temperature curves of $\varepsilon''_{33}(T,\nu)$ and $\varepsilon''_{11}(T,\nu)$ indicates that this transition is strongly smeared out (it starts near $T_{\rm f}$ and finishes at T_0).

The temperature $T_{\rm f}$, in the vicinity of which the proton freezing begins, is estimated by different methods. The EPR studies on paramagnetic Tl^{2+} impurity ions [24–26], whose spectrum is sensitive to structural transformations, in the RADP crystals show that the energy levels of these ions are gradually split by local fields with lowering temperature. This confirms the existence of a significant static random field in $Rb_{1-x}(NH_4)_xH_2PO_4$.

The chaotic static electric fields governed by the piezoelectric interactions and static elastic strains are believed [27] to be formed by chaotic substitutional disorder of ions of different radii. It has been shown that these fields act, mainly, on the lattice polarization along the c-axis and on the configurations with two protons near the "upper" or "lower" (with respect to the c-axis) oxygen atoms. It is shown that in addition to these chaotic fields and pseudospin-pseudospin interactions with a random sign, a chaotic local anisotropy should be taken into account. The difference in the symmetry of "upper" or "lower" and lateral proton configurations and peculiarities of the proton-lattice interactions can lead to coexistence of the long-range order with the glass state or paraelectric state.

The temperature dependence of the spin-lattice relaxation time for protons of NH_4 ionic groups in $Rb_{0.65}(NH_4)_{0.35}H_2PO_4$ was studied using the NMR method in [28]. In these compounds such a dependence has a minimum at ~ 180 K, associated with the start of proton freezing and with

the formation of hydrogen bonds between the NH_4 and PO_4 groups. In [29] the relaxation time of ^{31}P in $Rb_{1-x}(ND_4)_xD_2PO_4$ for different compositions was measured; a similar minimum in its temperature dependence was obtained near 170 K.

The X-ray structural studies revealed [30] a deviation of the lattice constants in $Rb_{1-x}(NH_4)_xH_2PO_4$ from the Debye approximation below a certain temperature $T_f(x) \sim 90$ K; these deviations increase with an increasing ammonium concentration. Despite the changes in the lattice constants, these compounds remain tetragonal. Below $T_f(x)$ in the proton glass phase composition region, a diffuse X-ray scattering increases [30–32]. This is particularly notable near the boundary between the ferroelectric and glass phases [32]. Possibly, this is related to the formation of some heterogeneous structure, that is, to coexistence of two phases.

In the obtained in [33, 34] Raman spectra of $Rb_{1-x}(ND_4)_xD_2PO_4$ ($x = 0.5$ and 0.25) some lines split below $T_f \sim 200$ K, due to of the non-equivalency of PO_4 groups (some of them are surrounded by Rb^+, while the others by ND_4^+). In the Raman spectra of $Rb_{0.3}(NH_4)_{0.7}H_2PO_4$ the orientational vibrations of NH_4^+ ions are revealed [35], indicating the formation of the $PO_4 - NH_4^+$ bonds and of the proton glass. The temperature dependence of the position of the peak, corresponding to the ν_2 vibrations of the PO_4 tetrahedra, has a characteristic break near $T_f \sim 100$ K. This break is related to the start of the proton freezing and their attaching to the PO_4 tetrahedra. A similar break was revealed in [36] for $K_{1-x}(NH_4)_xH_2PO_4$ ($x = 0.32, 0.53$) and in [37] for $Rb_{1-x}(NH_4)_xH_2AsO_4$ ($x = 0.35$).

The Edwards-Anderson parameter, which at moderately low temperatures is approximately proportional to the widths of various spectral lines, gradually increases with temperature lowering. This indicates that the transition to the proton glass state is smeared out. Thus, the NMR spectral line for $Rb_{1-x}(ND_4)_xD_2PO_4$ at different x [38, 39] and the NQR line for $Rb_{0.5}(NH_4)_{0.5}H_2PO_4$ [40] widen at lowering temperature, and the intensity of elastic neutron scattering from $Rb_{0.38}(ND_4)_{0.62}D_2PO_4$ increases [41].

Below T_0 the system becomes non-ergodic. The temperature T_0 is estimated by approximation of the experimental data for the dielectric permittivities at low temperatures. In [11] using the results of dielectric measurements and the following phenomenological expression for the longitudinal dielectric susceptibility

$$\chi(T,\nu) = \chi_0(T) \cdot \int_0^\infty \mathrm{d}\ln\tau \cdot \frac{g(\tau,T)}{1 - i2\pi\nu\tau},$$

the distribution function of relaxation times $g(\tau,T)$ was analyzed. In the time range $\tau \approx [\tau_0, \tau_c]$ the function $g(\tau,T)$ was qualitatively approximated by a rectangular distribution with the critical relaxation time τ_c. The best fit to the experimental data for $x = 0.35$ was obtained using the Vogel-Fulcher law

$$\tau_c = \tau_0 \exp\left(\frac{E_c}{T - T_0}\right), \qquad T_0 = 8.74 \text{ K}, \qquad E_c = 268 \text{ K},$$
$$\nu_0 = 1/2\pi\tau_0 = 3.49 \cdot 10^{12} \text{ Hz}.$$

At $T = T_0$ the maximal relaxation time becomes infinite. In [10] using the measured dielectric permittivities of $Rb_{0.5}(ND_4)_{0.5}D_2PO_4$ the value of $T_0 \approx 32$ K was obtained.

In [42] it has been shown that for $Rb_{0.53}(ND_4)_{0.47}D_2PO_4$ the spectrum of the distribution function $g(\tau,T)$ consists of two wide lines; with decreasing temperature from 55 K down to 35 K a fast intensity redistribution from smaller times to larger ones takes place. These results are interpreted within a model of dynamically correlated domains [43, 44], which form a system of classical dipoles. At the freezing temperature, part of them form an infinite percolation cluster. In this model $T_0 = 0$ K (the Arrhenius law).

At low temperatures an essential role is, most likely, played by proton tunneling. This is indicated by the maximum on the temperature curve of the dielectric losses tangent in $Rb_{0.25}(NH_4)_{0.75}H_2PO_4$ [8] at $T \approx 0.2$ K, as well as by splitting of NMR spectral lines of $Rb_{0.56}(ND_4)_{0.44}D_2PO_4$ [45]. This means that deuteron motion is not completely frozen out. Tunneling lowers down T_0.

Polarization relaxation and non-ergodic processes in proton glasses $M_{1-x}(NW_4)_xW_2AO_4$ (M = Rb, K; W = H, D; A = P, As) were explored by the Monte-Carlo method in [46]. The following interactions were taken into account: 1) between protons in the "upper" or "lower", lateral (W_2AO_4), and Takagi (WAO_4 and W_3AO_4) configurations; 2) between protons via NH_4 ions, which in pure ammonium compounds render the state with lateral configurations the ground state; 3) proton-lattice interactions, arising as a displacement field, if one of the nearest neighbors is the alkali ion, whereas the other is the ammonium ion; 4) interactions with an external electric field. At a given temperature the average value of polarization was calculated; the total number of proton jumps was up to 10^7 for each temperature. The temperature variation of polarization at heating in zero external field (P_{ZFH} with the initial value of $P_{\mathrm{ZFH}}(T=0)=P_{\mathrm{i}}$) and at heating in non-zero field (P_{FH} with the initial $P_{\mathrm{FH}}(T=0)=0$) was approximated by the following dependences

$$P_{\mathrm{ZFH}} = P_{\mathrm{i}} \cdot \exp\left[-\left(T/T_{\mathrm{e}}\right)^{\gamma}\right]; \qquad P_{\mathrm{FH}} = P_{\mathrm{f}} \cdot \left(1-\exp\left[-\left(T/T_{\mathrm{e}}\right)^{\gamma}\right]\right).$$

At small fields $T_{\mathrm{e}} \simeq T_{\mathrm{Slater}}0.53$, $\gamma = 6$, where the non-ergodicity temperature T_{e} is introduced. At small fields, when the temperature is raised to $T_{\mathrm{Slater}}0.38$ the relations $P_{\mathrm{ZFH}} \simeq P_{\mathrm{i}}$, $P_{\mathrm{FH}} \simeq 0$ hold, that is, at low temperatures the system is in the non-ergodic state.

Little attention has been paid to the investigation of a temperature dependence of specific heat of these systems in the glass phase region. We have come across a single paper [47], where it has been shown that the molar specific heat C(T) of $Rb_{1-x}(NH_4)_xH_2PO_4$ at $x = 0.7$ and $x = 0.74$ increases monotonously with temperature. Near 60 K the curve $C(T)$ is somewhat convex upwards. This convexity is most likely related to the protonic contribution to the specific heat, which is difficult to separate from the lattice contribution.

The ferroelectric phase composition region

In this region at high temperatures the q_{EA} parameter obtained from the NQR linewidths in $Rb_{1-x}(NH_4)_xH_2AsO_4$ with $x = 0.01$, 0.02 [48] and NMR linewidths in $Rb_{1-x}(ND_4)_xD_2PO_4$ [39] with $x = 0.22$ is different from zero. This indicates a partial proton freezing at high temperatures.

With lowering temperature, the transition to the ferroelectric phase takes place at $T_{\mathrm{c}}(x)$; in this phase a spontaneous polarization P_{s} exists. Unfortunately, the experimental data for P_{s} and q_{EA} are very limited, except for the case of $x = 0$. At $x = 0$, P_{s} has a jump at $T_{\mathrm{c}}(x)$. The temperature $T_{\mathrm{c}}(x)$ is maximal at $x = 0$ and decreases with increasing x, whereas the jump in P_{s} disappears (as observed in $Rb_{1-x}(NH_4)_xH_2AsO_4$ at $x = 0.08$ [18]), and the phase transition is smeared out. The temperature $T_{\mathrm{c}}(x)$ can be also determined from the NMR data. Thus, in [49] using the NMR method it has been established that the temperature dependence of the spin-lattice relaxation time of ^{87}Rb ions in $Rb_{1-x}(ND_4)_xD_2PO_4$ has a minimum at $T_{\mathrm{c}}(x)$.

The transverse dielectric permittivity $\varepsilon'_{11}(T,\nu)$ of the $Rb_{1-x}(NH_4)_xH_2PO_4$ type compounds in the ferroelectric phase composition region is somewhat smaller than in the glass phase region. It gradually increases at lowering temperature, then has a rounded maximum at $T_{\mathrm{c}}(x)$, and rapidly decreases to a certain constant value below $T_{\mathrm{c}}(x)$. At even lower temperature $T_{\mathrm{g}}(x)$ (inflection point), the permittivity $\varepsilon'_{11}(T,\nu)$ decreases to a minimal value. At the same time $\varepsilon''_{11}(T,\nu)$ has two maxima at $T_{\mathrm{c}}(x)$ and $T_{\mathrm{g}}(x)$. The same behavior was experimentally detected also for $\varepsilon'_{11}(T,\nu)$ and $\varepsilon''_{11}(T,\nu)$ in $Rb_{1-x}(NH_4)_xH_2PO_4$ [50], $Rb_{1-x}(ND_4)_xD_2PO_4$ [12], $Rb_{1-x}(NH_4)_xH_2AsO_4$ [16, 18, 51, 52], and $K_{1-x}(NH_4)_xH_2PO_4$ [53].

The longitudinal permittivity $\varepsilon'_{33}(T,\nu)$ of the $Rb_{1-x}(NH_4)_xH_2PO_4$ type compounds in the ferroelectric phase composition region also has a rounded peak at $T_{\mathrm{c}}(x)$, but its height is by two orders of magnitude larger than that of $\varepsilon'_{11}(T,\nu)$ and larger than in the glass phase composition region. It becomes larger and sharper with lowering x. Such a behavior of $\varepsilon'_{33}(T,\nu)$ was observed in $Rb_{1-x}(NH_4)_xH_2PO_4$ [3], $Rb_{1-x}(NH_4)_xH_2AsO_4$ [17], and $K_{1-x}(NH_4)_xH_2PO_4$ [22, 23, 54, 55].

In samples with smaller x the transition to the ferroelectric phase takes place at higher temperatures than in samples with higher x. Smearing of the transition to the ferroelectric phase is associated with fluctuations of ammonium concentration. Such an explanation is confirmed by the data of [56], where in the neutron diffraction patterns of $Rb_{0.9}(ND_4)_{0.1}D_2AsO_4$ the intensity

maxima characteristic of the paraelectric and of the ferroelectric phase were shown to coexist in a certain temperature range (7–10 K). This fact indicates coexistence of the two phases.

The presence of low-temperature peaks of $\varepsilon''_{11}(T,\nu)$ and $\varepsilon''_{33}(T,\nu)$ at $T_{\rm g}(x)$ in the ferroelectric phase composition region is related to coexistence of the ferroelectric and glass phases. Such a coexistence was revealed by measurements of $\varepsilon''_{11}(T,\nu)$ in $Rb_{1-x}(NH_4)_xH_2PO_4$ at $x = 0.15$ and 0.17 [50], $Rb_{1-x}(NH_4)_xH_2AsO_4$ [16, 18, 51, 57], $K_{1-x}(NH_4)_xH_2PO_4$ [53], $Rb_{0.96}(ND_4)_{0.04}D_2AsO_4$ [53, 58]. It is believed that in the ferroelectric phase composition region, the samples have small inclusions, in which the concentration of NH_4 is characteristic of the glass phase composition region. These inclusions at the temperature $T_{\rm g}(x)$ undergo a transition to the proton glass state. With lowering x the temperature $T_{\rm g}(x)$ decreases. This is associated with a decrease of the dimensions and correlation length of the clusters, where the transition to the glass state takes place; as a result, at low x the system dynamics is faster than at x close to the glass phase composition region.

In [57] the imaginary part of the permittivity $\varepsilon''_{11}(T,\nu)$ and the Cole-Cole curves were measured at different frequencies for low concentrations $x = 0$; 0.01; 0.05; 0.1 in $Rb_{1-x}(NH_4)_xH_2AsO_4$ and $Rb_{1-x}(ND_4)_xD_2AsO_4$. At $x = 0.05$; 0.1 a coexistence of the low-temperature proton glass phase and non-uniform ferroelectric phase has been detected below $T_{\rm g}(\nu,x)$. From the Cole-Cole curves a presence of the relaxation time distribution below $T_{\rm g}(\nu,x)$ is evident.

In [18] the temperature dependences of spontaneous polarization of $Rb_{1-x}(NH_4)_xH_2AsO_4$ and $Rb_{1-x}(ND_4)_xD_2AsO_4$ (at $x = 0.0$; 0.08), as well as transverse permittivities ε'_a (T, 1 kHz) (for $x = 0.0$; 0.08; 0.4 in $Rb_{1-x}(NH_4)_xH_2AsO_4$ and $x = 0.0$; 0.08; 0.28 in $Rb_{1-x}(ND_4)_xD_2AsO_4$) were measured. It has been shown that at $x = 0.08$ in the temperature range between $T_{\rm g}(x)$ and $T_{\rm c}(x)$ the sample polarization is proportional to the contribution of the so-called lost dielectric response

$$P_{\rm sd}(T) = P_{\rm so}\frac{\Delta\varepsilon'_{a1}(T)}{\varepsilon'_a(T,x=0.4)}\,; \qquad \Delta\varepsilon'_{a1}(T) = \varepsilon'_a(T,x=0.4) - \varepsilon'_a(T,x=0.08).$$

This indicates a presence of proton glass inclusions in the ferroelectric matrix at $x = 0.08$.

Antiferroelectric phase composition region

In this region the high-temperature proton glass phase exists at high temperatures, since the $q_{\rm EA}$ parameter obtained from the NMR linewidths in the $Rb_{1-x}(ND_4)_xD_2PO_4$ system is different from zero and increases with decreasing temperature [39, 59].

At lowering temperature, a phase transition to the antiferroelectric phase takes place at $T_{\rm N}(x)$. The transition temperature $T_{\rm N}(x)$ is maximal at $x = 1$, decreases with lowering x, and vanishes at a certain critical value of x, where the glass phase composition region begins. The obtained in [35] temperature dependence of the Raman scattering line, corresponding to ν_2 vibrations of PO_4 tetrahedra in $Rb_{1-x}(NH_4)_xH_2PO_4$ crystals at $x = 0.8$, has two bends at 130 K and 65 K. The first bend corresponds to $T_{\rm f}(x)$ and to the start of the proton freezing on the O–H…O bonds, just like in the glass phase composition region. The second bend corresponds to the transition to antiferroelectric phase at $T_{\rm N}(x)$, because below $T_{\rm N}(x)$ the frequency ν_2 increases due to the formation of the NH_4–PO_4 clusters. In [35] the two bends are also observed in the ferroelectric phase composition region at $x = 0.2$: the first one at $T_{\rm f}(x)$, the second one at $T_{\rm c}(x)$.

Using the experimental data for transverse dielectric permittivity of $Rb_{1-x}(NH_4)_xH_2PO_4$ [3, 4], $Rb_{1-x}(ND_4)_xD_2PO_4$ [12], $Rb_{1-x}(NH_4)_xH_2AsO_4$ [17], and $K_{1-x}(NH_4)_xH_2PO_4$ [19, 22, 60] it has been established that $\varepsilon'_{11}(T,\nu)$ in antiferroelectric phase composition region at $T > T_{\rm N}(x)$, just like in the glass and ferroelectric phase composition region, increases with lowering temperature, but the value of $\varepsilon'_{11}(T,\nu)$ here is somewhat larger. Near $T_{\rm N}(x)$ a fast decrease of $\varepsilon'_{11}(T,\nu)$ takes place, which at $x \to 1$ transforms into a break. At $T < T_{\rm N}(x)$ $\varepsilon'_{11}(T,\nu)$ is much smaller than at $T > T_{\rm N}$ and slightly decreases with lowering temperature. At x close to the glass phase composition region this decrease slows down, whereas the maximum of $\varepsilon'_{11}(T,\nu)$ at $T_{\rm N}(x)$ becomes rounded, that is, the phase transition is smeared out.

As has been shown in [60], $\varepsilon_{33}(T,\nu)$ in $K_{1-x}(NH_4)_xH_2PO_4$ at $x = 0.8$ and 0.9 is qualitatively similar to $\varepsilon_{11}(T,\nu)$, but twice smaller. This is the only experimental measurement of $\varepsilon_{33}(T,\nu)$ in the antiferroelectric phase composition region, except for the case $x = 1$.

In the antiferroelectric part of the phase diagram, the coexistence of deuteron glass and antiferroelectric phases in $Rb_{1-x}(ND_4)_xD_2AsO_4$ at ($x = 0.39$, 0.55, 0.69) was revealed [61] using the measured temperature and frequency dependences of $\varepsilon_{11}(T,\nu)$. This coexistence is indicated by a weak frequency dispersion of the temperature dependence of permittivity at $T \leqslant 100$ K (it is by two orders of magnitude smaller than in the region with the deuteron glass phase only at $x = 0.28$).

In [62] by the example of the $Rb_{1-x}(NH_4)_xH_2AsO_4$ system, a possibility of phase coexistence (of PE – dynamically disordered paraelectric phase, PG – structurally disordered proton glass state, FE – ferroelectric, and AFE – antiferroelectric phases) in this type of compounds is explored. Experimental evidence for this coexistence at different x is presented.

The temperature dependence of specific heat in the antiferroelectric phase composition region, as shown in [47] for $Rb_{1-x}(NH_4)_xH_2PO_4$ at $x = 0.79$ and 0.89, has two peaks: at T_N and a much lower one at a few degrees below T_N. The second peak remains unexplained. Considering the fact that the obtained results were not explained by their authors, and that a too high peak of the specific heat for these values of x was obtained, we can assume that these data are possibly unreliable.

Unfortunately, for all compositions and for both dielectric permittivities the experimental data obtained in different papers are in a poor agreement. Let us consider here examples of such discrepancies. It should be noted that $\varepsilon_{11}(T,\nu)$ and $\varepsilon_{33}(T,\nu)$ were measured at different frequencies. However, these frequencies are low enough, so the dielectric permittivity hardly varies with frequency in this temperature range.

In $Rb_{1-x}(NH_4)_xH_2PO_4$ at $x = 0.25$ (ferroelectric phase), $T = 60$ K $\varepsilon'_{33}(T,\nu) \approx 340$ as measured in [2] at ν=1 kHz and $\varepsilon'_{33}(T,\nu) \approx 250$ as measured in [3] at ν=300 Hz. In [2] and [7] at $T = 60$ K and close compositions in the proton glass phase $x = 0.4$ and 0.4 and frequencies ν=1 kHz and 12 kHz, respectively, it was obtained that $\varepsilon'_{33}(T,\nu) \approx 140$ and $\varepsilon'_{33}(T,\nu) \approx 65$, respectively, that is a nearly two-fold difference. The measured in [2] (1 kHz) and [6] (50 kHz) $\varepsilon'_{11}(T,\nu)$ for $x = 0.5$ is about 40% higher than measured in [3] (10 kHz); for $x = 0.7$ the measured in [2] (1 kHz) $\varepsilon'_{11}(T,\nu)$ is about 30% larger than measured in [3] (10 kHz) and [4] (70 kHz); whereas $\varepsilon'_{11}(T,\nu)$ at $x = 0.43$ [7] (12 kHz) is about 80% smaller than found in [2] (1 kHz) at a very close composition $x = 0.4$. In the system $Rb_{1-x}(ND_4)_xD_2PO_4$ with $x = 0.4$ (proton glass phase composition region) $\varepsilon'_{11}(T,\nu)$ obtained in [7] (12 kHz) is about twice smaller than in [14] (116 Hz).

In $Rb_{1-x}(NH_4)_xH_2AsO_4$ $\varepsilon'_{11}(T,\nu)$ found in [18] (1 kHz) for $x = 0.4$ (proton glass phase) is about 20% smaller, whereas that found in [17] (10 kHz) for $x = 0.44$ is about 10% smaller than that measured in [15] (30 kHz) for $x = 0.35$; in [17] $\varepsilon'_{11}(T,\nu)$ decreases with decreasing x. In $K_{1-x}(NH_4)_xH_2PO_4$ at $x = 0.39$ (proton glass phase) $\varepsilon'_{33}(T,\nu)$ measured in [21] (20 Hz) is about twice larger than measured at $x = 0.32$ in [20] (0.1 Hz), even though $\varepsilon'_{33}(T,\nu)$ in [20] strongly increases with lowering x.

Lots of other experimental data are available, which disagree within 10%. Such discrepancies can be explained by errors in measurements of $\varepsilon_{11}(T,\nu)$ and $\varepsilon_{33}(T,\nu)$, as well as by an incorrect determination of x. For example, the concentration of ammonium x in $K_{1-x}(NH_4)_xH_2PO_4$ depends non-linearly on its concentration in a solution during the sample growth [36].

The temperatures $T_g(x)$, corresponding to the maximum of $\varepsilon''_{11}(T,\nu)$ (inflection point of $\varepsilon'_{11}(T,\nu)$), obtained in different experiments are also different. Thus, for $Rb_{0.5}(ND_4)_{0.5}D_2PO_4$ T_g=59 K [12] at ν=1 kHz and T_g=53 K [9] at ν=10 kHz, and both in [12] and [9] $T_g(x)$ increases with frequency.

The data for the temperatures T_c in the ferroelectric phase composition region are also contradictory. Thus, T_c of $Rb_{1-x}(NH_4)_xH_2AsO_4$ determined from the maximum of $\varepsilon'_{33}(T,\nu)$ in [17] are about 10 K larger than T_c determined from the maximum of $\varepsilon'_{11}(T,\nu)$ in [16]. This means that the value of x is either overestimated in [17] or underestimated in [16].

Similar situation is observed for the experimental data for $\varepsilon'_{11}(T,\nu)$ in the antiferroelectric phase composition region. The values of $\varepsilon'_{11}(T,\nu)$ for $Rb_{1-x}(NH_4)_xH_2PO_4$ at $x = 0.9$ measured in [4] at cooling are by 20% larger than at heating and by about 10% larger than those obtained in [3]. The value of $\varepsilon'_{11}(T,\nu)$ measured in [60] for $K_{1-x}(NH_4)_xH_2PO_4$ at $x = 0.8$ is almost three times smaller than that found in [19].

Unfortunately, the experimenters who measured tensors of the dielectric permittivity did not comment on the discrepancies between their results and the previous measurements. We think that the major origin of these discrepancies is the difficulty of growing identical samples for a given x, because in these samples there are regions with different x. In spite of the quantitative differences, the qualitative behavior of the experimental curves of dielectric permittivities of the $Rb_{1-x}(NH_4)_xH_2PO_4$ type compounds is approximately the same. Therefore, very important are theoretical studies of these compounds.

1.2. Theoretical studies of the $Rb_{1-x}(NH_4)_xH_2PO_4$ compounds

From the point of view of a theoretical description, the $Rb_{1-x}(NH_4)_xH_2PO_4$ type compounds, which in a certain composition region can undergo a transition to the proton glass state, are quite similar to the magnetic compounds with a spin glass phase. Therefore, we can use the theoretical methods developed for the spin glass models. A detailed description of the proton glasses, however, is not possible within the spin glass models, since these models do not take into account the random electric fields and the real crystal structure of proton glasses.

In [63, 64] the Ising model in a transverse field with proton tunneling was explored. In [63] the interaction constants $J_{ij} = \pm J$ were taken to be different from zero only for the nearest neighbors. In [64], as in the Sherrington-Kirkpatrick model [65], J_{ij} are long-range ones and fluctuate with the Gaussian distribution. Calculations performed therein in the mean field approximation have shown that in both cases tunneling lowers down the temperatures of the transitions between the paraelectric and glass phases T_g ($q_{EA} \neq 0$ below T_g), as well as between the paraelectric and ferroelectric phase T_c or antiferroelectric phase T_N.

In [45, 66, 67] the Ising model in a transverse field Ω_i with a random internal longitudinal field h_i

$$H = -\frac{1}{2}\sum_{i,j} J_{ij} S_i^z S_j^z - \sum_i \Omega_i S_i^x - \sum_i (E + h_i) S_i^z, \tag{1.1}$$

was explored, where E is a uniform external field. Gaussian distributions are used for the random infinite range interactions with ($\langle J_{ij}^2 \rangle_c = x(1-x) \cdot \mathrm{const}(i-j)$) and random deformational field h_i ($\langle h_i \rangle = 0, \langle h_i^2 \rangle \sim x(1-x)$). In [66] within the replica symmetric approach, a system of equations for unknown p, q, r

$$p = \langle S_\alpha^z \rangle_n, \qquad q = \langle S_\alpha^z S_\beta^z \rangle_n, \qquad r = \left\langle (S_\alpha^z)^2 \right\rangle_n \underset{\Omega \to 0}{\longrightarrow} 1, \qquad n \to 0,$$

as well as expressions for the free energy, susceptibility χ, instability line of the replica symmetric solution (Almeida-Thouless line) are obtained and explored. Here α, β numerate the replicas, n is the total number of the replicas. It is shown that the temperature of the transition to the glass phase T_g exists only at $\langle h_i^2 \rangle_c = 0$ and corresponds to the peak on the temperature curve of $\chi(T)$. The random internal field ($\langle h_i^2 \rangle_c \neq 0$) leads to the occurrence of the proton glass-like state at any temperature above T_g ($q_{EA} > 0$, $q_{EA} \underset{T\to\infty}{\longrightarrow} 0$) and smoothes the peak in the temperature curve of $\chi(T)$. The distribution function of the local fields $P(h) = \langle \delta(h - h_i - \sum_j J_{ij} S_j) \rangle$ was calculated at $\Omega_i = 0$. Its shape at high temperatures is close to the Gaussian one, whereas at lowering temperature or increasing $\langle h_i^2 \rangle_c$ it transforms into a two-peak curve with a minimum at $h = 0$. Such a shape of $P(h)$ qualitatively agrees with the experimentally observed shape of EPR [24] and NMR [68] spectral lines. The temperature dependence of q_{EA} calculated within the model [66] well agrees with the second moment of the distribution function of the EPR [24] and NMR [39, 68] spectral lines. In [25, 69] for the model with Hamiltonian (1.1) at $\Omega_i = 0$, using the Glauber equation, a shape of the EPR line was calculated (a single-peak one at high temperatures and a two-peak one at low temperatures) that agrees well with the experiment in a wide temperature range ($T = [10\ K, 150\ K]$). For this model, as shown in [45], $q_{EA} \to 1$ at $\Omega_i = 0$, $T \to 0$. In the presence of tunneling ($\Omega_i \neq 0$) $q_{EA} < 1$ at all temperatures, which means an incomplete freezing.

In [67] the order parameter m and the parameter q_{EA} for the model with Hamiltonian (1.1) are calculated by the replica method, and the phase diagrams at different values of the transverse

field and of the random field dispersion are constructed. Since in the presence of random fields $q_{\rm EA} > 0$ at all T, the temperature of transition to the glass phase $T_{\rm g}(x)$ here is introduced as a temperature below which the replica-symmetry solution is instable, that is, the replica symmetry is broken, and the system is in non-ergodic state. It is established that the random fields decrease the temperatures $T_{\rm g}$, $T_{\rm c}$, and $T_{\rm N}$ and widen the glass phase region. It has been shown that between the glass and ferroelectric phases there exists a region where $m \neq 0$, and the replica symmetric solution is unstable; this region is called the region of coexistence of glass and ferroelectric phases.

If in (1.1) the distribution function of the fields $h_{\rm i}$ consists of two Gaussians, then a critical point appears on the phase boundary between the ferroelectric and paraelectric phases, whereas the transition between the ferroelectric and paraelectric phases becomes the first order one [70].

In [71] a dynamic generalization of the static approach of [66] has been presented. The $Rb_{1-x}(ND_4)_xD_2PO_4$, $Rb_{1-x}(ND_4)_xD_2AsO_4$ compounds described by the Hamiltonian

$$H = -\frac{1}{2}\sum_{i,j} J_{ij} S_i^z S_j^z - \sum_{\rm i} (E + h_{\rm i})\, S_i^z - g \sum_{i,k} \left(b_k + b_{-k}^{+}\right) S_i^x, \tag{1.2}$$

$$\langle J_{ij}\rangle \Big/ \sqrt{N} = J_0 = (1-2x)J, \qquad \left\langle J_{ij}^2 \right\rangle_{\rm c} \Big/ N = \Delta = 4x\cdot(1-x)J^2, \qquad \left\langle h_{\rm i}^2 \right\rangle_{\rm c} = \Delta_h$$

are considered. Here an interaction of the pseudospins with the phonon thermostat is introduced into the Ising model Hamiltonian. This leads to the Debye-type relaxation [71]

$$\varepsilon(\nu) = 1 + \frac{\beta}{4\pi}\frac{1 - \left\langle th^2\left(\beta h(\xi)\right)\right\rangle_\xi}{1 + i2\pi\nu\tau}, \qquad h(\xi) = \xi\Delta/2J^2\sqrt{q + 4\Delta_h/J^2} + J_0 p,$$

where polarization and the Edwards-Anderson parameter p, q obey the following system of equations

$$p = \int\limits_{-\infty}^{\infty} \frac{{\rm d}\xi}{\sqrt{2\pi}} \exp\left(-\frac{\xi^2}{2}\right) th\left[\beta h(\xi)\right], \qquad q = \int\limits_{-\infty}^{\infty} \frac{{\rm d}\xi}{\sqrt{2\pi}} \exp\left(-\frac{\xi^2}{2}\right) th^2\left[\beta h(\xi)\right].$$

For the relaxation time a phenomenological Arrhenius-like expression is assumed

$$\tau^{-1} \approx \int\limits_{-\infty}^{\infty} {\rm d}t\left[\langle b(t)b(0)\rangle + \langle b(0)b(t)\rangle\right] \sim \tau_0^{-1}\cdot {\rm e}^{-E/T}, \qquad E \approx 100\ {\rm K}.$$

A quantitative comparison of the obtained results with experiment was performed for the temperature behavior of the $\varepsilon''(\nu)$ peak only. It yielded

$$\varepsilon''_{\rm theor}(\nu_{\rm p}) = 0.027T - 0.10;$$

$$\varepsilon''_{\rm exp}(\nu_{\rm p}) = 0.04T - 0.57\left(Rb_{0.7}(ND_4)_{0.3}D_2AsO\right);$$

$$\varepsilon''_{\rm exp}(\nu_{\rm p}) = 0.11T - 3.411\left(Rb_{0.6}(ND_4)_{0.4}D_2PO_4\right).$$

It is claimed that the proposed simple approach can be useful for the description of dielectric properties of deuteron glasses. However, the relaxation theory of deuterated mixtures [71] based on this model does not yield a correct frequency dependence of the dielectric permittivity.

The drawback of the above described calculations based on the Ising model with transverse field and random longitudinal field is that they do not take into account the real structure of the $Rb_{1-x}(NH_4)_xH_2PO_4$ type compounds. Also, the interactions considered therein are long-range ones (of the Sherrington-Kirkpatrick type), whereas in the real systems the major role is played by the nearest neighbor interactions.

The first theory of the $Rb_{1-x}(NH_4)_xH_2PO_4$ mixtures that takes into account its real structure has been proposed in [72]. A pseudospin Hamiltonian was used to describe the energy levels of protons near the PO_4 groups; the critical lines $T_{\rm c}(x), T_{\rm N}(x)$ (an expansion over the order parameter

$1/N \sum_{i=1}^{N} \langle S_i \rangle)$ and $T_{\rm g}(x)$ (an expansion over $1/N \sum_{i=1}^{N} (\langle S_i \rangle)^2$) were found in the cluster approach. A qualitative description of the experimentally observed phase diagram was obtained.

Later the cluster approach was used in [73, 74]. Thus, in [73] for the description of the $Rb_{1-x}(NH_4)_xH_2PO_4$ a pseudospin model was proposed that takes into account the configurational energy of the cluster of hydrogen bonds near a PO_4 group and a long-range interaction W

$$H_{\rm cl} = \frac{V}{4}\left(S_1S_2 + S_2S_3 + S_3S_4 + S_4S_1\right) + \frac{U}{4}\left(S_1S_3 + S_2S_4\right) - \sum_{i=1}^{4}\left(\varphi_{{\rm cl},i} + W\langle S_i\rangle\right)S_i\,.$$

Here $\varphi_{{\rm cl},i}$ are the cluster fields that take into account the interactions of i-th hydrogen bond with protons of the neighboring tetrahedra and are determined from the condition of the extremum of the free energy for the mixture of different phases. The Hamiltonian parameters U, V are related to the two lowest levels of the hydrogen cluster in $RDP(\varepsilon_0', \varepsilon_1')$ and ADP $(\varepsilon_0, \varepsilon_1)$ as

$$U = \varepsilon_1'/2, V = \frac{1}{4}\left(\varepsilon_0' + 2\varepsilon_1'\right), \qquad U = \frac{1}{2}\left(\varepsilon_0 + \varepsilon_1\right)_1, \qquad V = \frac{1}{4}\left(\varepsilon_0 + 2\varepsilon_1\right).$$

The free energy is presented as a sum of the energies of three phases

$$F = p_+F(\varepsilon_0 < 0, W = 0) + p_0F(\varepsilon_0 = 0, W = 0) + p_-F(\varepsilon_0 > 0, W \neq 0)$$

with the probabilities p_+ for the ferroelectric phase, p_- for the antiferroelectric phase, and p_0 for the neutral phase.

It is believed that the state of each tetrahedron is formed by the six ionic positions (Rb or NH_4). Two of these six positions are the closest; therefore, the ferroelectric (antiferroelectric) state of the tetrahedron is formed if they are occupied with Rb (NH_4). In other situations a neutral state is formed. From the analysis of the free energy expansion over the parameters $\langle S_1\rangle + \langle S_3\rangle\,; \langle S_1\rangle - \langle S_3\rangle$ the regions of ferroelectric ($0 < x < 0.2$ at $T = 0$) and antiferroelectric ($0.75 < x < 1$ at $T = 0$) phases on the phase diagram are found that are close to experimental.

This model was used to describe the diagram of the state in the proton glass region ($0.2 < x < 0.75$ at $T = 0$) in [74]. Here the replica symmetric approximation was used in averaging the system free energy with a parameter, being an analog of the Edwards-Anderson parameter $q = \langle S_{f\alpha}S_{f\beta}\rangle\,(\alpha, \beta$ are the replica numbers). Analytical expressions for the partition function $L(n, q)$ and temperature of the glass transition $T_{\rm g}(n)$ (when $q = 0$) are found for the number of replicas n=2, 3, 4. For $T_{\rm g}(n)$ an expression is found for an arbitrary n. Hence, an expression $T_{\rm g}$ was obtained

$$\left(\frac{kT_{\rm g}}{\langle h^2\rangle}\right)^2 = \frac{1}{8}\frac{1 + 2\exp(-2\langle\varepsilon(x)\rangle/kT_{\rm g})}{\left(1 + 2\exp(-\langle\varepsilon(x)\rangle/kT_{\rm g})\right)^2}\,, \qquad T_{\rm g} = \lim_{n\to 0} T_{\rm g}(n).$$

Thus, no consistent approach to the description of all states of these compounds has been presented in [73, 74].

An original approach to the description of thermodynamical properties of proton glasses has been proposed in [75–77]. The model Hamiltonian contains terms responsible for the ferroelectric ordering along the Z axis (S^z-components of the classical spin) and for the antiferroelectric ordering (S^x-components). Restricting the consideration by the quadratic in the Hamiltonian terms at averaging the system free energy over the concentrations by the replica method, in the replica symmetric approximation, a system of equations was obtained for the parameters of ferroelectric p and antiferroelectric ξ ordering, as well as parameters of the short-range ordering g_z, g_x (correlation between the nearest dipole moments)

$$p = \langle\langle S_{i1}^z\rangle\rangle_{\rm c} = \langle\langle S_{i2}^z\rangle\rangle_{\rm c}\,, \qquad \xi = \langle\langle S_{i1}^x\rangle\rangle_{\rm c} = -\langle\langle S_{i2}^x\rangle\rangle_{\rm c}\,,$$
$$g_z = \langle\langle S_{i1}^zS_{i2}^z\rangle\rangle_{\rm c}\,, \qquad g_x = \langle\langle S_{i1}^xS_{i2}^x\rangle\rangle_{\rm c}\,.$$

Here 1, 2 are the sublattices of the site i; $\langle\ldots\rangle_{\rm c}$ means configurational averaging. The constructed phase diagram for $Rb_n(NH_4)_{1-n}H_2AsO_4$ qualitatively agrees with experiment. At high temperatures ($T \geqslant 210$ K) $p = 0$, $\xi = 0$, whereas for $g_{z,1}$, $g_{x,1}$ there exist single solutions that correspond to

the paraelectric region. The proton glass region is associated with the appearance of other solutions for g_z, g_x at $p = 0$, $\xi = 0$ (at low temperatures the maximal number of solutions is equal to 5). Fluctuations of the dipole moments are described by the averages amongst the dipole moments of the nearest spins g_z, g_x. The self-correlations of the dipole moments of the $\langle\langle S^z_{i1} S^z_{i1}\rangle\rangle_c$ type, measured in EPR or NMR experiments as the Edwards-Anderson parameter, are not taken into account in this approach. We believe that such correlations are more important than the correlations between the neighboring tetrahedra. Fluctuations of the deformational internal field, that can be estimated from the temperature dependence of the Edwards-Anderson parameter, are not taken into account in this approach either.

Hence, a theoretical description of thermodynamic and dielectric properties of hydrogen bonded compounds of the $Rb_{1-x}(NH_4)_xH_2PO_4$ type which can undergo a transition into the proton glass state, that would take into account the structural peculiarities and different types of interactions, is still a complicated and unsolved problem in statistical physics. Particularly it concerns a microscopic description of the dynamical properties of these mixtures. The temperature curves of the real and imaginary parts of the longitudinal and transverse dielectric permittivities at different frequencies have to be described. Of particular interest the possibility is to explore the low-temperature curves of the imaginary parts of dielectric permittivity at low frequencies.

In [78–81] a theory of static characteristics of model proton glasses with an arbitrary range of competing interactions has been proposed. In [82, 83] a similar approach has been used for the description of some thermodynamic characteristics and transverse dielectric permittivity of hydrogen bonded $Rb_{1-x}(ND_4)_xD_2PO_4$ and $Rb_{1-x}(NH_4)_xH_2AsO_4$ compounds, in which an essential role in the formation of energy levels is played by the proton short-range correlations. The goal of the present paper is to calculate the thermodynamic characteristics, the longitudinal and transverse dielectric permittivities of these compounds at different temperatures, concentrations, and frequencies, as well as to determine their phase diagrams.

2. Thermodynamic properties of the $Rb_{1-x}(NH_4)_x H_2PO_4$ type compounds

It is well known, that for description of thermodynamic characteristics and dielectric properties (in a certain frequency range) of these crystals within the pseudospin-phonon model, the ionic variables can be excluded in the static approximation ([84, 85]). The system description is then performed within the framework of a pseudospin model with renormalized moments of hydrogen bonds $\vec{d}_{f,\alpha}$ ($\alpha = +$ for RDP, $\alpha = -$ for ADP)

$$\vec{d}_{1\alpha} = (d^x_\alpha, 0, d^z_\alpha), \qquad \vec{d}_{3\alpha} = (-d^x_\alpha, 0, d^z_\alpha), \qquad \vec{d}_{2\alpha} = (0, -d^y_\alpha, d^z_\alpha), \qquad \vec{d}_{4\alpha} = (0, d^y_\alpha, d^z_\alpha),$$
$$\vec{P}^{A(B)}_\alpha = \sum_{f\in A(B)} \vec{d}_{f,\alpha}\eta^{A(B)}_{f,\alpha}; \quad \eta^{A(B)}_{f,\alpha} = \langle S_{f,\alpha}\rangle^{A(B)}. \tag{2.1}$$

Here we introduced an effective dipole moment of a tetrahedron $\vec{P}_\alpha$; $\langle\ldots\rangle$ is the conventional Gibbs' thermodynamic average; summation $f = A(B)$ is carried out over the bonds, on which the protons order close to the given tetrahedron $A(B)$. For RDP the tetrahedron polarization can have two opposite values along the c axis, when two protons are ordered close to the upper edge of the tetrahedron ($\eta_{\rm f} = \eta$) and close to the lower one ($\eta_{\rm f} = -\eta$)

$$\eta_{\rm f} = \eta \Rightarrow \vec{P}^{A(B)}_+ = (0, 0, 2d^z_+\eta), \qquad \eta_{\rm f} = -\eta \Rightarrow \vec{P}^{A(B)}_+ = (0, 0, -2d^z_+\eta). \tag{2.2}$$

For ADP–$NH_4H_2PO_4$ the primitive cell is twice as large as for RDP, and in addition to "A", "B" tetrahedra it contains "A'", "B'" tetrahedra. Since their polarizations are opposite to those of "A", "B", the total cell polarization is zero:

$$\begin{aligned} -\eta^A_{1,-} = -\eta^A_{2,-} = \eta^A_{3,-} = \eta^A_{4,-} = \eta; \quad \vec{P}^A_- = -\vec{P}^{A'}_- = (-d^x_-\eta; +d^y_-\eta; 0),\\ -\eta^B_{1,-} = \eta^B_{2,-} = \eta^B_{3,-} = -\eta^B_{4,-} = \eta; \quad \vec{P}^B_- = -\vec{P}^{B'}_- = (-d^x_-\eta, -d^y_-\eta, 0). \end{aligned} \tag{2.3}$$

For an ADP-$NH_4H_2PO_4$ crystal the change of sign of $\eta^{A(B)}_{f,-}$ at transition to the "A'", "B'" tetrahedra can be taken into account as (here $\vec{n}$ the RDP primitive cell vector; $\vec{k}^z_*$ is the vector at the Brillouin zone boundary directed along Z)

$$\eta^{A(B)}_{nf,-} = \mathrm{e}^{\mathrm{i}\vec{n}\vec{k}^z_*} \cdot \eta^{A(B)}_{f,-}. \tag{2.4}$$

Hence, in the cases of both ADP and RDP we use a primitive cell with "A" and "B" tetrahedra.

Hamiltonian of a mixed $Rb_{1-x}(NH_4)_xH_2PO_4$ system can be written as

$$\begin{aligned} H(\{h\}) &= -\sum_{n,f}\left(\langle\vec{d}_{nf}\rangle_{\mathrm{c}}\cdot\left[\vec{E}+\vec{G}_n\right]\right)S_{nf}+\sum_n\left[H_A(n)+H_B(n)\right] \\ &\quad -\frac{1}{2}\sum_{n,f}\sum_{n',f'}J_{nf,n'f'}S_{nf}S_{n'f'}\,, \\ H_A(n) &= \frac{V_n}{4}\left(S_{n1}S_{n2}+S_{n2}S_{n3}+S_{n3}S_{n4}+S_{n4}S_{n1}\right) \\ &\quad +\frac{U_n}{4}\left(S_{n1}S_{n3}+S_{n2}S_{n4}\right)+\frac{\Phi_n}{16}S_{n1}S_{n2}S_{n3}S_{n4}\,. \end{aligned} \tag{2.5}$$

Here $S_{nf}=\pm1$ are spin operators describing the position of a proton on the $f=1,2,3,4$ hydrogen bond in the $\vec{n}$ cell at the R tetrahedron; $\vec{E}$ is an external uniform electric field; $\vec{G}_n$ is an internal random deformational field; $J_{nf,n'f'}$ is the long-range interaction between protons; $H_A(n), H_B(n)$ are the configurational energies of the "A", "B" tetrahedra. In this work we take into account two configurational states of a tetrahedron ($\alpha=+,-$):

$$V_\alpha=-\frac{1}{8}w_{1\alpha},\qquad U_\alpha=\frac{1}{8}\left(w_{1\alpha}-2\varepsilon_\alpha\right),\qquad \Phi_\alpha=\frac{1}{8}\left(w_{1\alpha}+2\varepsilon_\alpha-4w_\alpha\right),\qquad \alpha=+,-. \tag{2.6}$$

In the state $+$, the energy states of a tetrahedron are analogous to those in a pure RDP crystal with the ground state level ε_{s+}

$$\varepsilon_+=\varepsilon_{a+}-\varepsilon_{s+}\,,\qquad w_+=\varepsilon_{1+}-\varepsilon_{s+}\,,\qquad w_{1+}=\varepsilon_{o+}-\varepsilon_{s+}\,. \tag{2.7}$$

In the state $-$ (ADP) we use the same relations for V_α, U_α, Φ_α but with different values of ε_α, w_α, $w_{1\alpha}$.

In the case of a mixed $Rb_{1-x}(NH_4)_xH_2PO_4$ crystal, ionic positions are occupied by Rb with the probability $c_+=1-x$ and by NH_4 with the probability $c_-=x$. Hence, the distribution function of a strongly random energy parameter ε_α (and similarly for $w_\alpha, w_{1\alpha}$) can be qualitatively written as

$$p(\sigma)=(1-x)\delta(\sigma-\varepsilon_+)+x\delta(\sigma-\varepsilon_-)=c_+\delta(\sigma-\varepsilon_+)+c_-\delta(\sigma-\varepsilon_-). \tag{2.8}$$

A state of the dipole moment on the bond $\vec{d}_{f,\alpha\alpha_{\mathrm{f}}}$ is determined by the states $\alpha,\alpha_{\mathrm{f}}$ of two tetrahedra connected by this bond. In the mean field approximation over the bonds, the averaged over configurations moment of a tetrahedron $\left\langle\vec{P}^B\right\rangle_{\mathrm{c}}$ reads

$$\left\langle\vec{P}\right\rangle_{\mathrm{c}}\approx\sum_{f=1}^{4}\left\langle\vec{d}_{\mathrm{f}}\right\rangle_{\mathrm{c}}\bar{\eta}_{\mathrm{f}},\qquad \left\langle\vec{d}_{\mathrm{f}}\right\rangle_{\mathrm{c}}=\sum_\alpha\sum_\beta c_\alpha c_\beta\vec{d}_{f,\alpha\beta},\ \bar{\eta}_{\mathrm{f}}=\langle\langle S_{\mathrm{f}}\rangle\rangle_{\mathrm{c}}\,. \tag{2.9}$$

In the present work we consider only two realizations of the sets of averaged over configurations values of $\bar{\eta}_{\mathrm{f}}=\bar{\eta}$; $-\bar{\eta}^B_{1,-}=\bar{\eta}^B_{2,-}=\bar{\eta}^B_{3,-}=-\bar{\eta}^B_{4,-}=\bar{\eta}$, which correspond to ferroelectric and antiferroelectric ordering. This permits us to use the primitive cell of RDP with 2 tetrahedra and 4 hydrogen bonds. The mean free energy per primitive cell $\langle\mathbf{F}\rangle$ can then be written as

$$\begin{aligned} -\beta\langle\mathbf{F}\rangle &= -\sum_{f=1,\in A}^{4}\left\langle F^{(0)}_{\mathrm{f}}\right\rangle_{\mathrm{c}}+\left\langle F^{[0]}_A\right\rangle_{\mathrm{c}}+\left\langle F^{[0]}_B\right\rangle_{\mathrm{c}} \\ &\quad -\beta\sum_{f=1,\in A}^{4}\bar{\varphi}_{L,f}\left\langle F^{(1)}_{\mathrm{f}}\right\rangle_{\mathrm{c}}+\frac{\beta}{2}\sum_{f,f'=1,\in A}^{4}\left\langle J_{f,f'}(\vec{k}_*)\right\rangle_{\mathrm{c}}\left\langle F^{(1)}_{\mathrm{f}}\right\rangle_{\mathrm{c}}\left\langle F^{(1)}_{f'}\right\rangle_{\mathrm{c}}, \end{aligned} \tag{2.10}$$

where $\vec{k}_* = \vec{0}_*$ for ferroelectric ordering $\left\langle F_{\rm f}^{(1)}\right\rangle_{\rm c} = \left\langle F^{(1)}\right\rangle_{\rm c}$, $\vec{k}_* = \vec{k}_*^z$ for antiferroelectric ordering $-\left\langle F_1^{(1)}\right\rangle_{\rm c} = \left\langle F_2^{(1)}\right\rangle_{\rm c} = \left\langle F_3^{(1)}\right\rangle_{\rm c} = -\left\langle F_4^{(1)}\right\rangle_{\rm c} = \left\langle F^{(1)}\right\rangle_{\rm c}$. We use the following notations for the averages over different random fields of the single-particle $F_{\rm f}^{(0)}$ and cluster $F_{1234}^{[0000]}$ generating functions

$$\begin{aligned}
\left\langle F_{\rm f}^{(0)}\right\rangle_{\rm c} &= \left\langle F^{(0)}(\zeta_{\rm f})\right\rangle_{\rm c} = \left\langle F^{(0)}\left(\kappa_{\rm f}+\sigma+g_x+g_y+g_z\right)\right\rangle_{\sigma,\vec{g}} \\
&= \int\ldots\int {\rm d}\sigma R\left(\sigma,2q\right)\rho_t(g_x)\rho_t(g_y)\rho_z(g_z){\rm d}g_x{\rm d}g_y{\rm d}g_z F^{(0)}(\kappa_{\rm f}+\sigma+g_x+g_y+g_z)\,, \quad (2.11)\\
\left\langle F_A^{[0]}\right\rangle_{\rm c} &= \left\langle F_{1234}^{[0000]}\right\rangle_{\rm c} = \left\langle F^{[0000]}(\xi_1|\xi_2|\xi_3|\xi_4||R)\right\rangle_{\rm c} \\
&= \int\ldots\int\prod_{f=1}^{4}{\rm d}\sigma_{\rm f} R\left(\sigma_{\rm f},q\right)\rho(g_x)\rho(g_y)\rho(g_z){\rm d}g_x{\rm d}g_y{\rm d}g_z \\
&\quad\times\left\langle F^{[0000]}\left(\kappa_{cl,1}+\sigma_1+g_1|\ldots|\kappa_{cl,4}+\sigma_4+g_4||R\right)\right\rangle_{\{\sigma\},\vec{g},R}\,. \quad (2.12)
\end{aligned}$$

Here we introduce notations for the average values of cluster $\bar{\varphi}_{\rm f}$ and long-range $\bar{\varphi}_{\rm L,f}$ fields, and

$$\begin{aligned}
\kappa_{\rm f} &= h_{\rm f}+\bar{\varphi}_{L,f}+2\bar{\varphi}_{\rm f}\,, \qquad \kappa_{cl,f} = h_{\rm f}+\bar{\varphi}_{L,f}+\bar{\varphi}_{\rm f}\,, \qquad h_{\rm f} = \left(\left\langle\vec{d}_{\rm f}\right\rangle_{\rm c}\cdot\vec{E}\right)\,,\\
g_1 &= g_z-g_x\,, \qquad g_2 = g_z+g_y\,, \qquad g_3 = g_z+g_x\,, \qquad g_4 = g_z-g_y\,. \quad (2.13)
\end{aligned}$$

Averaging is performed over random cluster fields with dispersion q and over random deformational fields with dispersion $\langle G^2\rangle_{\rm c}$ for transverse and longitudinal field components

$$R\left(\sigma,q\right) = \frac{e^{-\frac{1}{2}\frac{\sigma^2}{q}}}{\sqrt{2\pi q}}\,, \qquad \rho\left(\sigma\right) = \frac{e^{-\frac{1}{2}\frac{\sigma^2}{\langle G^2\rangle_{\rm c}}}}{\sqrt{2\pi\langle G^2\rangle_{\rm c}}}\,, \qquad \langle G^2\rangle_{\rm c} = 4x(1-x)Q_G\,. \quad (2.14)$$

The expressions for the single-particle function $F_{\rm f}^{(0)}$ and its derivatives $F_{\rm f}^{(n)}$ are as follows

$$\begin{aligned}
F_{\rm f}^{(0)} &= \ln\left[2{\rm ch}\left(\beta\zeta_{\rm f}\right)\right]\,, \qquad F_{\rm f}^{(n)} = \partial^n/\partial(\beta\zeta_{\rm f})^n F_{\rm f}^{(0)}, \qquad F_{\rm f}^{(1)} = {\rm th}\left(\beta\zeta_{\rm f}\right)\,,\\
F_{\rm f}^{(2)} &= 1-\left(F_{\rm f}^{(1)}\right)^2, \qquad F_{\rm f}^{(3)} = -2F_{\rm f}^{(1)}F_{\rm f}^{(2)}, \qquad F_{\rm f}^{(4)} = -2F_{\rm f}^{(2)}\left[1-3\left(F_{\rm f}^{(1)}\right)^2\right]. \quad (2.15)
\end{aligned}$$

The cluster function $F_{1234}^{[0000]}$ and its derivatives $F_{1234}^{[n_1n_2n_3n_4]}$ read

$$\begin{aligned}
&F^{[0000]}(\xi_1|\xi_2|\xi_3|\xi_4||R) = \ln\left[0.5\cdot L(\xi_1,\xi_2,\xi_3,\xi_4||R_\alpha)\right]\,,\\
&F_{1234}^{[n_1n_2n_3n_4]} = \frac{\partial^{n_1}}{\partial(\beta\xi_1)^{n_1}}\cdots\frac{\partial^{n_4}}{\partial(\beta\xi_1)^{n_4}}F_{1234}^{[0000]}\,,\\
&F_{11}^{[1,1]} = F^{[2000]}(\xi_1|\xi_2|\xi_3|\xi_4||R) = 1-M_1^{[1]}M_1^{[1]},\\
&F_{12}^{[1,1]} = F^{[1100]}(\xi_1|\xi_2|\xi_3|\xi_4||R) = M_{12}^{[1,1]}-M_1^{[1]}M_2^{[1]},\\
&F_{13}^{[1,1]} = F^{[1010]}(\xi_1|\xi_2|\xi_3|\xi_4||R) = M_{13}^{[1,1]}-M_1^{[1]}M_3^{[1]},\\
&F_{14}^{[1,1]} = F^{[1001]}(\xi_1|\xi_2|\xi_3|\xi_4||R) = M_{14}^{[1,1]}-M_1^{[1]}M_4^{[1]},\\
&F_{ff'}^{[21]} = -2F_{\rm f}^{[1]}F_{ff'}^{[11]}, \quad F_{ff'}^{[21]} = -2F_{ff'}^{[11]}F_{f'}^{[1]},\\
&F_{ff'}^{[22]} = -2F_{ff'}^{[1,1]}\left[M_{ff'}^{[1,1]}-M_{\rm f}^{[1]}M_{f'}^{[1]}\right],\\
&M_1^{[1]} = L_{1234}^{[1000]}\Big/L_{1234}^{[0000]},\ldots M_4^{[1]} = L_{1234}^{[0001]}\Big/L_{1234}^{[0000]},\\
&M_{11}^{[1,1]} = L_{1234}^{[2000]}\Big/L_{1234}^{[0000]}\equiv 1,\ldots,M_{14}^{[1,1]} = L_{1234}^{[1001]}\Big/L_{1234}^{[0000]}, \quad (2.16)
\end{aligned}$$

$$\begin{aligned} 0.5L_{1234}^{[0000]} &= 0.5L(\xi_1,\xi_2,\xi_3,\xi_4||R_\alpha)=2a_\alpha ch(\beta\xi_1-\beta\xi_3)ch(\beta\xi_2-\beta\xi_4) \\ &\quad + ch(\beta\xi_1+\beta\xi_2+\beta\xi_3+\beta\xi_4)+d_\alpha ch(\beta\xi_1-\beta\xi_2+\beta\xi_3-\beta\xi_4) \\ &\quad +2b_\alpha\left[ch(\beta\xi_1+\beta\xi_3)ch(\beta\xi_2-\beta\xi_4)+ch(\beta\xi_1-\beta\xi_3)ch(\beta\xi_2+\beta\xi_4)\right], \\ a_\alpha &= \exp(-\beta\varepsilon_\alpha), \qquad b_\alpha=\exp(-\beta w_\alpha), \qquad d_\alpha=\exp(-\beta w_{1\alpha}). \end{aligned} \tag{2.17}$$

Here the partition function $0.5L\left(\{\xi\}\,||R_\alpha\right)$ is calculated with the cluster Hamiltonian

$$\begin{aligned} H_A(\{\xi\};S_1,S_2,S_3,S_4||R) &= H_A(\{0\};S_1,S_2,S_3,S_4||R)-\sum_{f=1}^{4}\xi_{\rm f}S_{\rm f}\,, \\ H_A(\{0\};S_1,S_2,S_3,S_4||R) &= \frac{V_\alpha}{4}\left(S_1S_2+S_2S_3+S_3S_4+S_4S_1\right)+\frac{U_\alpha}{4}\left(S_1S_3+S_2S_4\right) \\ &\quad +\frac{\Phi_\alpha}{16}S_1S_2S_3S_4\,. \end{aligned} \tag{2.18}$$

We shall use the same model dependence of the average eigenvalues of the long-range interaction matrix as for the dipole moment of a hydrogen bond:

$$\left\langle \nu_\mu(\vec{k}_*)\right\rangle_{\rm c}=\bar\nu_\mu(\vec{k}_*)=\sum_\alpha\sum_\beta c_\alpha c_\beta\nu_{\mu,\alpha\beta}(\vec{k}_*)\approx c_+^2\nu_{\mu,++}(\vec{k}_*)+c_-^2\nu_{\mu,--}(\vec{k}_*)+2c_+c_-\nu_{\mu,00}(\vec{k}_*). \tag{2.19}$$

For these values of $\vec{k}_*$ the long-range interaction matrix $\bar J_{f,f'}=\left\langle J_{f,f'}\left(\vec{k}_*\right)\right\rangle_{\rm c}$ and the unitary transformation matrix $\hat U=\{u_{\mu f}\}$ read

$$\hat U=\hat U^+=\frac{1}{2}\begin{pmatrix}1&1&1&1\\1&1&-1&-1\\1&-1&1&-1\\1&-1&-1&1\end{pmatrix}; \qquad \hat{\bar J}=\left\langle\hat J\right\rangle=\begin{pmatrix}\bar J_{11}&\bar J_{12}&\bar J_{13}&\bar J_{12}\\\bar J_{12}&\bar J_{11}&\bar J_{12}&\bar J_{13}\\\bar J_{13}&\bar J_{12}&\bar J_{11}&\bar J_{12}\\\bar J_{12}&\bar J_{13}&\bar J_{12}&\bar J_{11}\end{pmatrix};$$

$$\hat{\bar\nu}=\hat U\hat{\bar J}\hat U=\begin{pmatrix}\bar\nu_1&0&0&0\\0&\bar\nu_2&0&0\\0&0&\bar\nu_3&0\\0&0&0&\bar\nu_4\end{pmatrix}. \tag{2.20}$$

$$\bar\nu_1=\bar J_{11}+2\bar J_{12}+\bar J_{13}\,, \qquad \bar\nu_2=\bar\nu_4=\bar J_{11}-\bar J_{13}\,, \qquad \bar\nu_3=\bar J_{11}-2\bar J_{12}+\bar J_{13}\,. \tag{2.21}$$

From the condition of the free energy extremum we find an expression for the average $\bar\eta_{\rm f}=\langle\langle S_{\rm f}\rangle\rangle_{\rm c}$, reduced Edwards-Anderson parameter $Q_{\rm EA,f}$, and an equation for unknown quantities $\bar\varphi_{\rm L,f},\bar\varphi_{\rm f},q_{\rm f}$

$$\begin{aligned} \bar\eta_{\rm f} &= \left\langle F_{\rm f}^{(1)}\right\rangle_{\rm c}, \qquad Q_{{\rm EA},f}=q_{{\rm EA},f}-\bar\eta_{\rm f}^2, \qquad q_{{\rm EA},f}=1-\left\langle F_{\rm f}^{(2)}\right\rangle_{\rm c}, \\ \left\langle F_{\rm f}^{(1)}\right\rangle_{\rm c} &= \left\langle F_{\rm f}^{[1000]}\right\rangle_{\rm c}, \qquad \left\langle F_{\rm f}^{(2)}\right\rangle_{\rm c}=\left\langle F_{\rm f}^{[2000]}\right\rangle_{\rm c}, \qquad \bar\varphi_{L,f}=\sum_{f_1}^{4}\bar J_{ff_1}(\vec{k}_*)\bar\eta_{f_1}. \end{aligned} \tag{2.22}$$

In the absence of external field and for the ferroelectric ordering we obtain the following expressions for the free energy, for the average $\bar\eta=\bar\eta_{\rm f}$, reduced Edwards-Anderson parameter $Q_{\rm EA}=Q_{\rm EA,f}$ and for equations for $\bar\varphi_L,\bar\varphi,q$

$$\begin{aligned} &\bar\eta=\bar\eta_{\rm f}\,, \qquad \bar\varphi=\bar\varphi_{\rm f}\,, \qquad \bar\varphi_L=\bar\varphi_{L\,,f}\,, \qquad q=q_{\rm f}\,, \\ &-\beta\left\langle\mathbf{F}_F\right\rangle_{\rm c}=-4\left\langle F^{(0)}\right\rangle_{\rm c}+2\left\langle F_A\right\rangle_{\rm c}-4\beta\bar\varphi_L\left\langle F^{(1)}\right\rangle_{\rm c}+2\beta\bar\nu_1(\vec{0}_*)\left\langle F^{(1)}\right\rangle_{\rm c}^2, \\ &\bar\eta=\left\langle F^{(1)}\right\rangle_{\rm c}, \qquad Q_{\rm EA}=q_{\rm EA}-\bar\eta^2\,, \qquad q_{\rm EA,f}=1-\left\langle F^{(2)}\right\rangle_{\rm c}, \\ &\left\langle F^{(1)}\right\rangle_{\rm c}=\left\langle F^{[1000]}\right\rangle_{\rm c}, \qquad \left\langle F^{(2)}\right\rangle_{\rm c}=\left\langle F^{[2000]}\right\rangle_{\rm c}, \qquad \bar\varphi_L=\bar\nu_1(\vec{0}_*)\bar\eta. \end{aligned} \tag{2.23}$$

In the case of an antiferroelectric ordering in the absence of external field, the free energy, for the average $\bar{\eta} = -\bar{\eta}_1 = \bar{\eta}_2$, reduced Edwards-Anderson parameter $Q_{\rm EA} = Q_{\rm EA,f}$ and equations for $\bar{\varphi}_L, \bar{\varphi}, q$ read

$$\begin{aligned}
&\bar{\eta} = -\bar{\eta}_{1(4)} = \eta_{2(3)}, \qquad \bar{\varphi} = -\bar{\varphi}_{1(4)} = \bar{\varphi}_{2(3)}, \qquad \bar{\varphi}_L = -\bar{\varphi}_{L,1(4)} = \bar{\varphi}_{L,2(3)}, \qquad q = q_{\rm f},\\
&-\beta \left\langle \mathbf{F}_{AF} \right\rangle_{\rm c} = -4 \left\langle F^{(0)} \right\rangle_{\rm c} + 2 \left\langle F_A \right\rangle_{\rm c} - 4\beta\bar{\varphi}_L \left\langle F^{(1)} \right\rangle_{\rm c} + 2\beta\nu_2(\vec{k}^z_*) \left\langle F^{(1)} \right\rangle^2_{\rm c},\\
&\bar{\eta} = \left\langle F^{(1)} \right\rangle_{\rm c} = -\left\langle F^{(1)}_1 \right\rangle_{\rm c}, \qquad Q_{\rm EA} = q_{\rm EA} - \bar{\eta}^2, \qquad q_{{\rm EA},f} = 1 - \left\langle F^{(2)} \right\rangle_{\rm c},\\
&\left\langle F^{(1)} \right\rangle_{\rm c} = \left\langle F^{[0100]} \right\rangle_{\rm c}, \qquad \left\langle F^{(2)} \right\rangle_{\rm c} = \left\langle F^{[0200]} \right\rangle_{\rm c}, \qquad \bar{\varphi}_L = \bar{\nu}_2(\vec{k}^z_*)\bar{\eta}.
\end{aligned} \tag{2.24}$$

As numerical calculations for the free energy show, the antiferroelectric state is realized in the region close to the $x = 1-c \to 1$ limit; the ferroelectric state is realized in the region $1-x = c \to 1$, and a proton glass state ($\bar{\varphi} = \bar{\varphi}_L = 0, q > 0$) takes place at intermediate compositions.

The static susceptibility of the system reads ($v_{\rm e}$ is the cell volume)

$$\begin{aligned}
&\chi_{ab} = -\frac{1}{Tv_{\rm e}} \sum_{f,f'} \langle d^a_{\rm f} \rangle_{\rm c} \langle d^b_{f'} \rangle_{\rm c} \cdot \bar{\eta}'_{ff'} = -\frac{1}{Tv_{\rm e}} \sum_{\mu} \tilde{d}^a_\mu \tilde{d}^b_\mu \cdot \tilde{\eta}'_\mu\,,\\
&\bar{\eta}'_{ff'} = \frac{\partial \bar{\eta}_{\rm f}}{\partial(\beta h_{f'})}\,, \qquad \tilde{d}^a_\mu = \sum_{\rm f} u_{\mu f} \langle d^a_{\rm f} \rangle_{\rm c}\,, \qquad \tilde{\eta}'_\mu = \sum_{f,f'} u_{\mu f} u_{\mu f'} \bar{\eta}'_{ff'}\,.
\end{aligned} \tag{2.25}$$

Here we used the fact that after the unitary transformation with $\hat{U}$, the matrix of $\tilde{\eta}'_{\mu\mu'} = \delta_{\mu\mu'}\tilde{\eta}'_\mu$ correlators is diagonal for ferroelectric and antiferroelectric orderings, and

$$\begin{aligned}
&\tilde{\eta}'_1 = \bar{\eta}'_{11} + \bar{\eta}'_{12} + \bar{\eta}'_{13} + \bar{\eta}'_{14}\,, \qquad \tilde{\eta}'_2 = \bar{\eta}'_{11} + \bar{\eta}'_{12} - \bar{\eta}'_{13} - \bar{\eta}'_{14}\,,\\
&\tilde{\eta}'_3 = \bar{\eta}'_{11} - \bar{\eta}'_{12} + \bar{\eta}'_{13} - \bar{\eta}'_{14}\,, \qquad \tilde{\eta}'_4 = \bar{\eta}'_{11} - \bar{\eta}'_{12} - \bar{\eta}'_{13} + \bar{\eta}'_{14}.
\end{aligned} \tag{2.26}$$

In this work we shall explore temperature and composition dependences of the longitudinal $\varepsilon_{33}(T)$ and transverse $\varepsilon_{11}(T)$ permittivity of the system

$$\begin{aligned}
&\varepsilon_{aa}(T) = \varepsilon^0_{aa} + 4\pi\chi_{aa}(T), \qquad \varepsilon^0_{aa} = 1 + 4\pi\chi^0_{aa}, (a = 1,2,3),\\
&\chi_{33}(T) = -4\frac{1}{Tv_{\rm e}} \left(\langle d^z \rangle_{\rm c}\right)^2 \tilde{\eta}'_1(T), \quad \chi_{aa}(T) = -\frac{1}{Tv_{\rm e}} \left(\langle d^a \rangle_{\rm c}\right)^2 \left(\tilde{\eta}'_2(T) + \tilde{\eta}'_4(T)\right), \quad a = 1,2.
\end{aligned} \tag{2.27}$$

In order to find the quantities $\tilde{\eta}'_\mu$ occurring in the expression for the susceptibility, we differentiate $\bar{\eta}_{\rm f}$ and equation (2.22) for $\bar{\varphi}_{\rm L,f}, \bar{\varphi}_{\rm f}, q_{\rm f}$ with respect to the fields $\beta h_{f'}$ and obtain equations for $\bar{\eta}'_{ff'}$, $\bar{\varphi}'_{ff'}$, and $q'_{ff'}$

$$\begin{aligned}
&\left[1 - \left\langle \hat{F}^{(2)} \right\rangle_{\rm c} \beta\hat{\tilde{J}}(\vec{0})\right] \hat{\bar{\eta}}' = \left\langle \hat{F}^{(2)} \right\rangle_{\rm c} \left[1 + 2\beta\hat{\bar{\varphi}}'\right] + \frac{1}{2} \left\langle \hat{F}^{(2)} \right\rangle_{\rm c} \beta^2 2\hat{q}',\\
&\left[2\left\langle \hat{F}^{(2)} \right\rangle_{\rm c} - \left\langle \hat{F}^{[11]} \right\rangle_{\rm c}\right] \beta\hat{\bar{\varphi}}' + \frac{1}{2}\left[2\left\langle \hat{F}^{(3)} \right\rangle_{\rm c} - \left\langle \hat{F}^{[12]} \right\rangle_{\rm c}\right] \beta^2\hat{q}'\\
&\qquad = \left[-\left\langle \hat{F}^{(2)} \right\rangle_{\rm c} + \left\langle \hat{F}^{[11]} \right\rangle_{\rm c}\right] \left[1 + \beta\hat{\tilde{J}}(\vec{0})\hat{\bar{\eta}}'\right],\\
&\left[2\left\langle \hat{F}^{(3)} \right\rangle_{\rm c} - \left\langle \hat{F}^{[21]} \right\rangle_{\rm c}\right] \beta\hat{\bar{\varphi}}' + \frac{1}{2}\left[2\left\langle \hat{F}^{(4)} \right\rangle_{\rm c} - \left\langle \hat{F}^{[22]} \right\rangle_{\rm c}\right] \beta^2\hat{q}'\\
&\qquad = \left[-\left\langle \hat{F}^{(2)} \right\rangle_{\rm c} + \left\langle \hat{F}^{[21]} \right\rangle_{\rm c}\right] \left[1 + \beta\hat{\tilde{J}}(\vec{0})\hat{\bar{\eta}}'\right].
\end{aligned} \tag{2.28}$$

We multiply these equations by the unitary matrix $\hat{U}$ (2.20) from the left, rendering all the matrices in equations (2.28) diagonal or antidiagonal.

Let us explore the symmetry of the matrices in these equations in the case of antiferroelectric ordering (in the case of ferroelectric ordering all minus signs are changed to plus signs), as well as the form of the matrices after the unitary transformation

$$\langle \hat{F}^{(2n)} \rangle_{\rm c} = \langle F^{(2n)} \rangle_{\rm c} \cdot \hat{I}, \qquad \hat{\tilde{F}}^{(2n)} = \hat{U}^+ \cdot \langle F^{(2n)} \rangle_{\rm c} \cdot \hat{U} \equiv \langle \hat{F}^{(2n)} \rangle_{\rm c}\,, \tag{2.29}$$

$$\langle\hat{F}^{(2n+1)}\rangle_{\rm c} = \langle F^{(2n+1)}\rangle_{\rm c}\begin{pmatrix} 1 & 0 & 0 & 0\\ 0 & -1 & 0 & 0\\ 0 & 0 & -1 & 0\\ 0 & 0 & 0 & 1\end{pmatrix}; \quad \hat{\tilde{F}}^{(2n+1)} = \langle F^{(2n+1)}\rangle_{\rm c}\begin{pmatrix} 0 & 0 & 0 & 1\\ 0 & 0 & 1 & 0\\ 0 & 1 & 0 & 0\\ 1 & 0 & 0 & 0\end{pmatrix};$$

$$\hat{\bar{\varphi}}' = \begin{pmatrix} \bar{\varphi}'_{11} & \bar{\varphi}'_{12} & \bar{\varphi}'_{13} & \bar{\varphi}'_{14}\\ \bar{\varphi}'_{12} & \bar{\varphi}'_{11} & \bar{\varphi}'_{14} & \bar{\varphi}'_{13}\\ \bar{\varphi}'_{13} & \bar{\varphi}'_{14} & \bar{\varphi}'_{11} & \bar{\varphi}'_{12}\\ \bar{\varphi}'_{14} & \bar{\varphi}'_{13} & \bar{\varphi}'_{12} & \bar{\varphi}'_{11}\end{pmatrix}; \qquad \tilde{\bar{\varphi}}' = \hat{U}\hat{\bar{\varphi}}'\hat{U} = \begin{pmatrix} \tilde{\varphi}'_1 & 0 & 0 & 0\\ 0 & \tilde{\varphi}'_2 & 0 & 0\\ 0 & 0 & \tilde{\varphi}'_3 & 0\\ 0 & 0 & 0 & \tilde{\varphi}'_4\end{pmatrix}; \tag{2.30}$$

$$\tilde{\varphi}'_1 = \bar{\varphi}'_{11} + \bar{\varphi}'_{12} + \bar{\varphi}'_{13} + \bar{\varphi}'_{14};\ \tilde{\varphi}'_2 = \bar{\varphi}'_{11} + \bar{\varphi}'_{12} - \bar{\varphi}'_{13} - \bar{\varphi}'_{14};$$
$$\tilde{\varphi}'_3 = \bar{\varphi}'_{11} - \bar{\varphi}'_{12} + \bar{\varphi}'_{13} - \bar{\varphi}'_{14};\ \tilde{\varphi}'_4 = \bar{\varphi}'_{11} - \bar{\varphi}'_{12} - \bar{\varphi}'_{13} + \bar{\varphi}'_{14};$$

$$\hat{q}' = \begin{pmatrix} q'_{11} & -q'_{12} & -q'_{13} & q'_{14}\\ q'_{12} & -q'_{11} & -q'_{14} & q'_{13}\\ q'_{13} & -q'_{14} & -q'_{11} & q'_{12}\\ q'_{14} & -q'_{13} & -q'_{12} & q'_{11}\end{pmatrix}; \qquad \tilde{\hat{q}}' = \begin{pmatrix} 0 & 0 & 0 & \tilde{q}'_4\\ 0 & 0 & \tilde{q}'_3 & 0\\ 0 & \tilde{q}'_2 & 0 & 0\\ \tilde{q}'_1 & 0 & 0 & 0\end{pmatrix}; \tag{2.31}$$

$$\tilde{q}'_1 = q'_{11} - q'_{12} - q'_{13} + q'_{14},\ \tilde{q}'_2 = q'_{11} - q'_{12} + q'_{13} - q'_{14},$$
$$\tilde{q}'_3 = q'_{11} + q'_{12} - q'_{13} - q'_{14},\ \tilde{q}'_4 = q'_{11} + q'_{12} + q'_{13} + q'_{14}.$$

The averaged matrices of the second derivatives $\langle\hat{F}^{[11]}\rangle_{\rm c}; \langle\hat{F}^{[22]}\rangle_{\rm c}$ for the antiferroelectric phase are of the same symmetry as the matrix $\hat{\bar{\varphi}}'$, and the eigenvalues of these matrices $\tilde{F}^{[11]}_\mu; \tilde{F}^{[22]}_\mu$ are written as linear combinations similar to $\tilde{\varphi}'_\mu$. Symmetry of the matrix $\langle\hat{F}^{[21]}\rangle_{\rm c}$ is the same as of $\hat{q}'$; after the unitary transformation it becomes analogous to the antidiagonal matrix $\tilde{\hat{q}}'$ with the corresponding elements $\tilde{F}^{[21]}_\mu$. The matrix $\langle\hat{F}^{[12]}\rangle_{\rm c}$ is transposed to $\langle\hat{F}^{[21]}\rangle_{\rm c}$. After the unitary transformation and exclusion of the parameters $\tilde{\varphi}'_\mu, \tilde{q}'_\mu$ we obtain expressions for the correlators $\tilde{\eta}'_\mu$, entering the expression for the system susceptibility.

$$\tilde{\eta}'_\mu = -\left[D_\mu/B_\mu - \beta\bar{\nu}_\mu(\vec{0})\right]^{-1} \underset{\rm ProtonGlassState}{\longrightarrow} -\left[2/\tilde{F}^{[11]}_\mu - \left(1 - \langle F^{(1)}\rangle_{\rm c}\right)^{-1} - \beta\bar{\nu}_\mu(\vec{0})\right]^{-1}, \tag{2.32}$$
$$D_\mu = \left[2\langle F^{(2)}\rangle_{\rm c} - \tilde{F}^{[11]}_\mu\right]\left[2\langle F^{(4)}\rangle_{\rm c} - \tilde{F}^{[22]}_\mu\right] - \left[2\langle F^{(3)}\rangle_{\rm c} - \tilde{F}^{[12]}_\mu\right]\left[2\langle F^{(3)}\rangle_{\rm c} - \tilde{F}^{[21]}_\mu\right],$$
$$B_\mu = \bar{F}^{(2)}\cdot\tilde{F}^{[11]}_\mu\left[2\langle F^{(4)}\rangle_{\rm c} - \tilde{F}^{[22]}_\mu\right] + \langle F^{(2)}\rangle_{\rm c}\tilde{F}^{[12]}_\mu\tilde{F}^{[21]}_\mu - 2\left[\langle F^{(3)}\rangle_{\rm c}\right]^2\tilde{F}^{[11]}_\mu.$$

In the case of the ferroelectric ordering the matrices $\hat{\tilde{\eta}}', \hat{\tilde{\varphi}}', \hat{q}', \left\langle\hat{F}^{[nn']}\right\rangle_{\rm c}$ have the same symmetry. As a result, we obtain the same expression for $\tilde{\eta}'_\mu$, except that for the eigenvalues $\tilde{F}^{[12]}_\mu$ we have to use the linear combination like for $\tilde{\varphi}'_\mu$.

Let us note that dynamic susceptibility $\chi_{aa}(\nu, T)$ of the system is expressed via the dynamic eigenvalues $\tilde{\eta}'_\mu(\nu)$ as in the static case (2.27) after the replacement $\tilde{\eta}'_\mu \to \tilde{\eta}'_\mu(\nu)$. The expressions for $\tilde{\eta}'_\mu(\nu)$ are derived in [82].

3. Discussion

3.1. Optimal sets of model parameters

Using the obtained in previous sections expressions, let us evaluate the dielectric and thermal characteristics of the $Rb_{1-x}(ND_4)_xD_2PO_4$ and $Rb_{1-x}(NH_4)_xH_2AsO_4$ compounds and compare them with the corresponding experimental data. Values of the theory parameters should provide the best possible fit to the experiment.

Table 1. Parameters for $Rb_{1-x}(ND_4)_xD_2PO_4$.

tetrahedron state	ε_α K	w_α K	$\nu_{1,\alpha\alpha}(0)$ K	$\nu_{2,\alpha\alpha}(k^z)$ K	$\nu_{2,\alpha\alpha}(0)$ K
+(Ferro)	160	1100	22.76	25	20
0(Glass)	–	–	–44	40	–60
–(Antiferro)	–140	750	–40	67.44	–20

tetrahedron state	$d^z_\alpha(G), 10^{-18}$ esu·cm	$d^z_\alpha(F), 10^{-18}$ esu·cm	$d^x_\alpha(G), 10^{-18}$ esu·cm	$d^x_\alpha(F), 10^{-18}$ esu·cm
+(Ferro)	0.95	0.95	3.25	3.25
0(Glass)	1.7	0.9	3.55	1.0
–(Antiferro)	1.65	1.65	3.15	1.0

tetrahedron state	χ^0_{33}	χ^0_{11}	v_e 10^{-21}cm	$\sqrt{\langle G^2\rangle}$, K	$\tau^z_{0,\alpha}$, s 10^{-14}	$\tau^x_{0,\alpha}$, s 10^{-14}
+(Ferro)	0.8	0.8	0.209	–	2.0	3
0(Glass)	0.6	0.7	–	24.5	0.55	6
–(Antiferro)	0.34	0.58	0.211	–	6.0	3

The found sets of the model parameters for the mixtures $Rb_{1-x}(ND_4)_xD_2PO_4$ ($T_c(x=0) = 235$ K, $T_N(x=1) = 242$ K), $Rb_{1-x}(NH_4)_xH_2AsO_4$ ($T_c(x=0) = 110$ K, $T_N(x=1) = 216$ K) are presented in tables 1–4, respectively. The dashes in the tables mean that the given tetrahedron is averaged over two states only (without the neutral state 0 (Glass)).

Table 2. Parameters for $Rb_{1-x}(NH_4)_xH_2AsO_4$.

tetrahedron state	ε_α K	w_α K	$\nu_{1,\alpha\alpha}(0)$ K	$\nu_{2,\alpha\alpha}(k^z)$ K	$\nu_{2,\alpha\alpha}(0)$ K
+(Ferro)	60	500	9.83	5	5
0(Glass)	–	–	–15	22	–25
–(Antiferro)	–100	470	–80	75.19	5

tetrahedron state	$d^z_\alpha(G), 10^{-18}$ esu ·cm	$d^z_\alpha(F), 10^{-18}$ esu·cm	$d^x_\alpha(G), 10^{-18}$ esu·cm	$d^x_\alpha(F), 10^{-18}$ esu·cm
+(Ferro)	0.88	0.59	2.55	2.55
0(Glass)	1.2	0.59	3.2	3.2
–(Antiferro)	1.35	1.35	3.15	1.0

tetrahedron state	χ^0_{33}	χ^0_{11}	v_e 10^{-21}cm	$\sqrt{\langle G^2\rangle}$, K	$\tau^z_{0,\alpha}$, s 10^{-14}	$\tau^x_{0,\alpha}$, s 10^{-14}
+(Ferro)	0.5	0.7	0.2236	–	60	7
0(Glass)	0.45	1.1	–	10	60	7
–(Antiferro)	0.3	0.7	0.2275	–	60	7

3.2. Spontaneous polarization

The calculated temperature curves of spontaneous polarization for $Rb_{1-x}(ND_4)_xD_2PO_4$ and $Rb_{1-x}(NH_4)_xH_2AsO_4$ compounds along with the available experimental data are shown in figure 2. The calculated dependences $P_s(T)$ well describe the experimental data at $x = 0$. With increasing x the theory predicts a decrease of spontaneous polarization, until it completely vanishes at the concentration corresponding to the transition into the glass phase composition region. The temper-

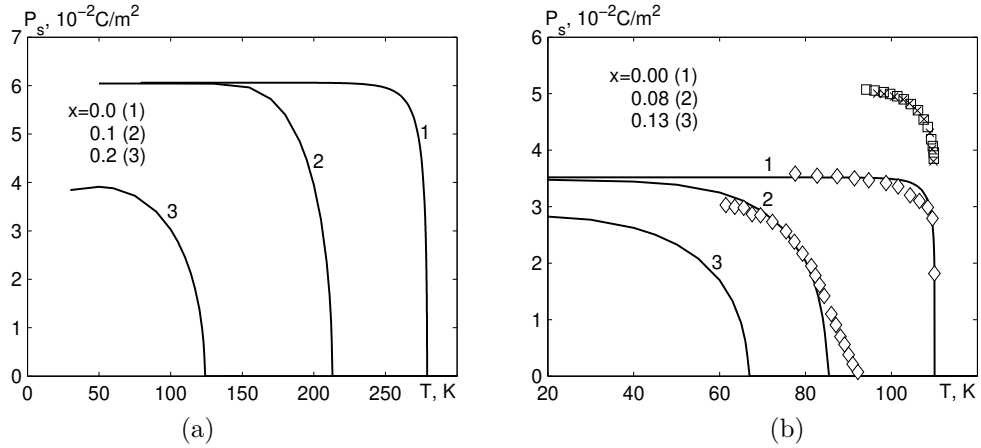

Figure 2. Temperature behavior of spontaneous polarization of a tetrahedron $P_s^z = P^z/v_e$ in the ferroelectric region of the phase diagram for $Rb_{1-x}(ND_4)_xD_2PO_4$ (a) at x: 0.0 – 1; 0.1 – 2; 0.2 – 3; for $Rb_{1-x}(NH_4)_xH_2AsO_4$ (b) at x: 0.0 – 1, ◇ [18], ▫ [86], × [87]; 0.08 – 2; 0.13 – 3.

atures, at which the spontaneous polarization arises in the ferroelectric phase, or the spontaneous sublattice polarization arises in the antiferroelectric phase, at different x yield the $T_c(x)$ or $T_N(x)$ dependences, respectively.

Let us note that at small x the saturation polarization is almost independent of x (curves 1 and 2 for all compounds), even though the order parameter $\bar{\eta}(x,T)$ at small T decreases with x. As seen from equation (2.9) the polarization is determined by the product $\langle d^z \rangle_c \bar{\eta}$. For all explored compounds the following relation is obeyed $d_-^z(F) > d_+^z(F)$, and the average $\langle d^z \rangle$ increases with x, whereas the low-temperature polarization of a tetrahedron is almost independent of x. With increasing x the parameter $\bar{\eta}$ rapidly decreases at low T, which leads to a rapid decrease of saturation polarization.

3.3. Molar specific heat

The experimental points for the proton contribution ΔC_p to the specific heat of the considered systems should be determined by subtracting the lattice contribution from the measured specific heat; the lattice contribution in the phase transition region is approximated by a linear dependence. The proposed theory, as seen in figures 3–4, properly describes the temperature dependence of proton contribution to the molar specific heat of the $Rb_{1-x}(ND_4)_xD_2PO_4$ and $Rb_{1-x}(NH_4)_xH_2AsO_4$ compounds at $x = 0$ and $x = 1$. At compositions other than $x = 0$ or $x = 1$ the theory predicts a decrease of the jump of specific heat at T_c and T_N and its vanishing at x in the proton glass composition region. To answer the question about the validity of the proposed theory for the $Rb_{1-x}(NH_4)_xH_2PO_4$ type systems, further experimental investigation of the temperature dependences of specific heat of these crystals in a wide composition range are required.

3.4. The reduced Edwards-Anderson parameter

The reduced Edwards-Anderson parameter $Q_{EA}(T)$ of the $Rb_{1-x}(NH_4)_xH_2PO_4$ type compounds is different from zero at all temperatures and concentrations x, except for $x = 0$ and $x = 1$ (figure 5). Let us note that the temperature and composition dependences of $Q_{EA}(T)$ are similar for all compounds. The parameter $Q_{EA}(T)$ has a rounded peak at transition from the high-temperature paraelectrical phase to the ferroelectric phase, whereas it rapidly falls to zero at transition to the antiferroelectric phase. The parameter $Q_{EA}(T)$ is the largest in the proton glass phase composition region and increases with decreasing temperature. For $Rb_{1-x}(ND_4)_xD_2PO_4$ at $x = 0.22$ the theoretical curve 3 (figure 5 (b)) satisfactorily describes the experimental data of [39]. At the same time, at $x = 0.44$ our calculations agree with the data of [68], but the obtained values

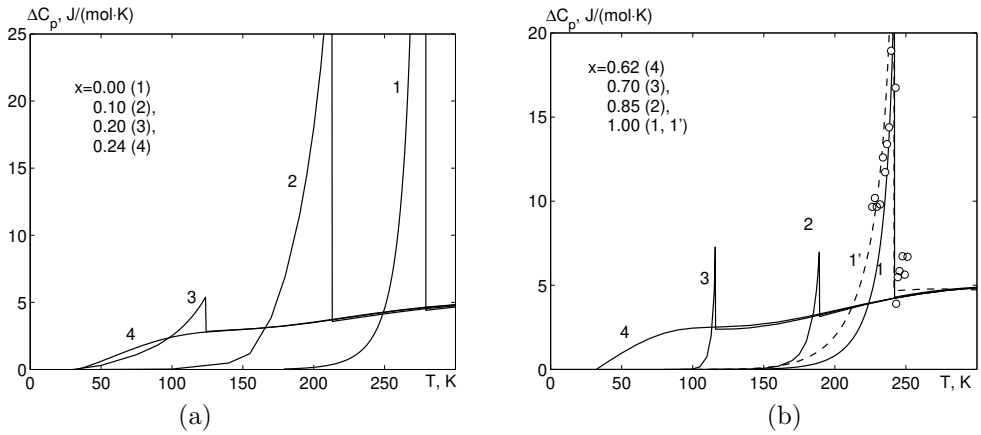

Figure 3. Temperature behavior of the proton contribution $\Delta C_{\rm p}$ to the specific heat of $Rb_{1-x}(ND_4)_xD_2PO_4$ in the ferroelectric (a) region of the phase diagram at x: 0.0 – 1; 0.1 – 2; 0.2 – 3; 0.24 – 4; and in the antiferroelectric (b) region at x: 1.0 – 1, ○ [88], 1'[85]; 0.85 – 2; 0.7 – 3; 0.62 – 4.

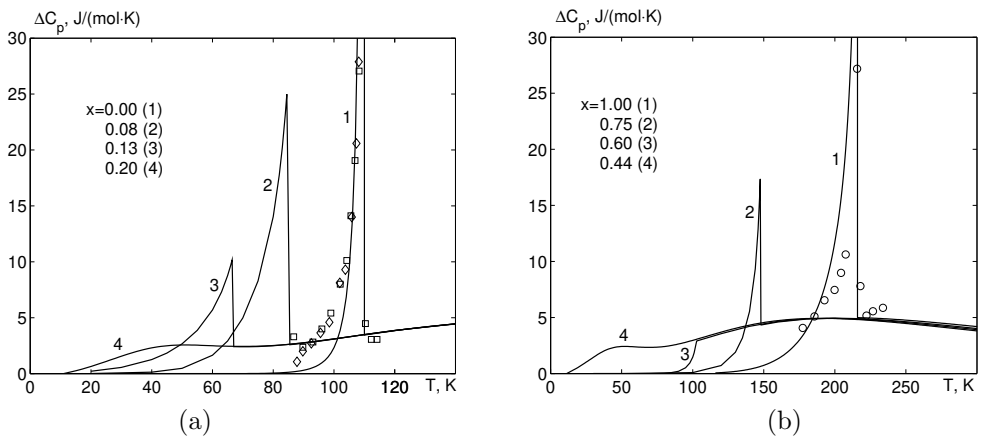

Figure 4. Temperature behavior of the proton contribution $\Delta C_{\rm p}$ to the specific heat of $Rb_{1-x}(NH_4)_xH_2AsO_4$ in the ferroelectric (a) region of the phase diagram at x: 0.0 – 1, □ [86], ◇ [87]; 0.08 – 2; 0.13 – 3; 0.2 – 4; and in the antiferroelectric (b) region at x: 1.0 – 1, ○ [89]; 0.75 – 2; 0.6 – 3; 0.45 – 4.

are lower than those of [39] both for $x = 0.44$ and $x = 0.22$. We believe that this can be explained by an incorrectly determined composition x of the samples in [39]. Unfortunately, no experimental data for $Q_{\rm EA}(T)$ were available for $Rb_{1-x}(NH_4)_xH_2AsO_4$.

3.5. Longitudinal dielectric permittivity

The temperature dependence of transverse permittivity for the $Rb_{1-x}(ND_4)_xD_2PO_4$ and $Rb_{1-x}(NH_4)_xH_2AsO_4$ compounds was explored in previous papers [82, 83].

In figures 6, 7 we show the temperature curves of the longitudinal static permittivity of $\varepsilon'_{33}(T,0)$ ($\varepsilon'_{33}(T,0) = \varepsilon_{33}(T)$) of the $Rb_{1-x}(ND_4)_xD_2PO_4$ and $Rb_{1-x}(NH_4)_xH_2AsO_4$ compounds at different x along with the experimental data for $\varepsilon'_{33}(T,\nu)$ at low frequencies.

An essential difference between these quantities arises only in the proton glass composition region and at temperatures below the maximum of $\varepsilon'_{33}(T,\nu)$. Here $\varepsilon'_{33}(T,\nu)$ even at small ν always tends to ε^0_{33}, whereas the theoretical static permittivity $\varepsilon'_{33}(T,0)$ at $T \to 0$ tends to a certain finite value, larger than ε^0_{33}. At high temperatures the static and dynamic permittivities practically coin-

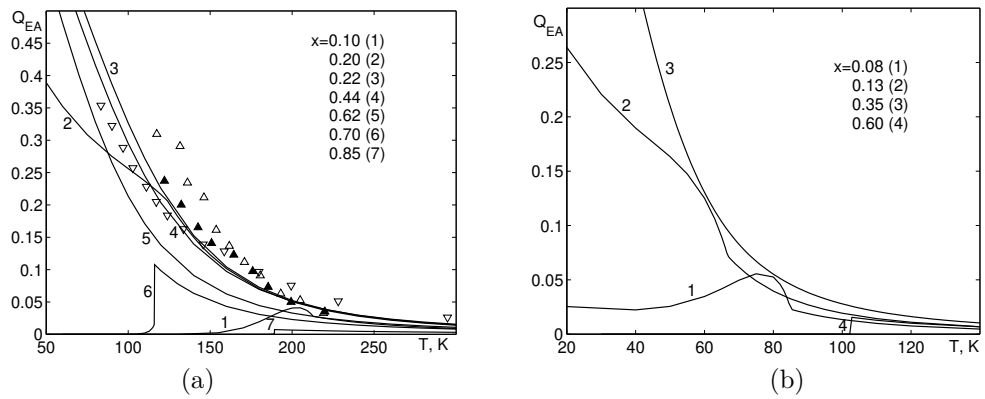

Figure 5. The temperature dependence of the reduced Edwards-Anderson parameter $Q_{\rm EA}$ for $\mathrm{Rb}_{1-x}(\mathrm{ND}_4)_x\mathrm{D}_2\mathrm{PO}_4$ at different x: 0.1 – 1; 0.2 – 2; 0.22 – 3, ▲ [39]; 0.44 – 4, △ [39], ▽ [68]; 0.62 – 5; 0.7 – 6; 0.85 – 7; for $Rb_{1-x}(NH_4)_xH_2AsO_4$ at different x: 0.08 – 1; 0.13 – 2; 0.35 – 3; 0.6 – 4.

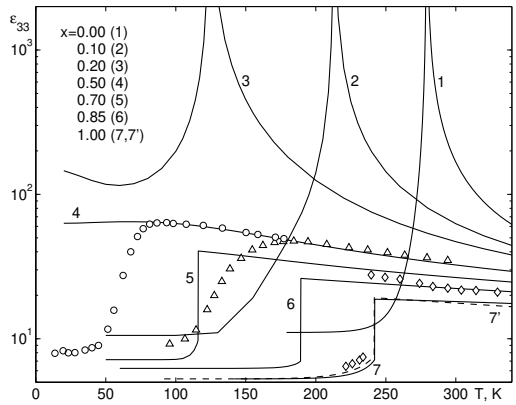

Figure 6. The temperature dependence of the longitudinal permittivity $\varepsilon'_{33}(T,\nu)$ of $\mathrm{Rb}_{1-x}(\mathrm{ND}_4)_x\mathrm{D}_2\mathrm{PO}_4$ at different x: 0.0 – 1; 0.1 – 2; 0.2 – 3; 0.5 – 4, ○[9] (10 kHz), △ [10] (10 GHz); 0.7 – 5; 0.85 – 6; 1.0 – 7, 7' [85], ◇ [90].

cide; this permits us to talk about qualitative agreement or disagreement between the theoretical curves for $\varepsilon'_{33}(T,0)$ and experimental points for $\varepsilon'_{33}(T,\nu\neq 0)$.

In figure 6 we show the temperature dependence of the longitudinal permittivity $\varepsilon'_{33}(T,\nu)$ of $\mathrm{Rb}_{1-x}(\mathrm{ND}_4)_x\mathrm{D}_2\mathrm{PO}_4$ at different x. At $x = 0.0$ (1), 0.1 (2), 0.2 (3) (ferroelectric composition region) no experimental data were available. The experimental points for $x = 0.5$ ○ [9] (10 kHz), Δ [10] (10 GHz) correspond to the glass phase composition region (static curve 4). At $x = 0.7$ (5), $x = 0.85$ (6), $x = 1.0$ (7) we have the antiferroelectric ordering region. Let us note that for $x = 1.0$ the agreement with experiment for $\varepsilon_{33}(T)$ (curve 7') would be slightly better if a different set of the model parameter values was used [85].

In figure 7 the calculated longitudinal static permittivity $\varepsilon_{33}(T)$ for $\mathrm{Rb}_{1-x}(\mathrm{NH}_4)_x\mathrm{H}_2\mathrm{AsO}_4$ is compared with the experimental data for $\varepsilon'_{33}(T,\nu\neq 0)$ for different compositions x at low frequencies ν. In the ferroelectric phase composition region ($x = 0$; 0.08; 0.13) the static theory correctly describes the parts of the curves above $T_{\rm c}(x)$ as well as the position of the maximum of $\varepsilon'_{33}(T,\nu\to 0)$, but their values in the vicinity of the peak are much larger than experimental ones. This peak can be smeared out and lowered down, if we take into account macroscopic fluctuations of concentration x as well as the piezoelectric effect. In the proton glass composition region the theory and experiment coincide quantitatively at temperatures above the peak of $\varepsilon'_{33}(T,\nu)$. At

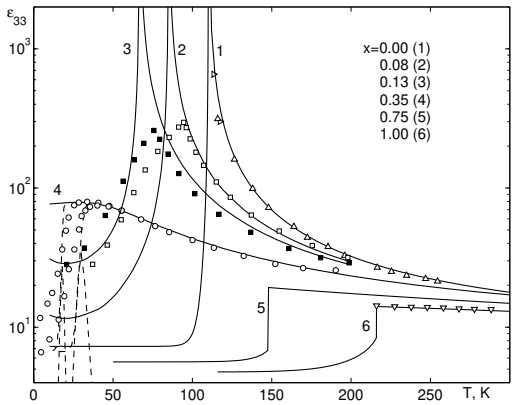

Figure 7. The temperature dependence of the longitudinal permittivity $\varepsilon'_{33}(T,\nu)$ of $Rb_{1-x}(NH_4)_xH_2AsO_4$ at different x: 0.0 – 1, △ [91], ▷ [92]; 0.08 – 2, ▫ [17] (1 MHz); 0.13 – 3, ■ [17] (1 MHz); 0.35 – 4, ○ [15] (1 Hz, 30 KHz); 0.75 – 5; 1.0 – 6, ▽ [93]. The dashed lines correspond to the theoretical curves for $x = 0.35$, ν=1 Hz, 30 kHz.

$x = 0.0$, 1.0, considering the dispersion of experiment points, we can talk about a quantitative agreement of theoretical results with experimental points.

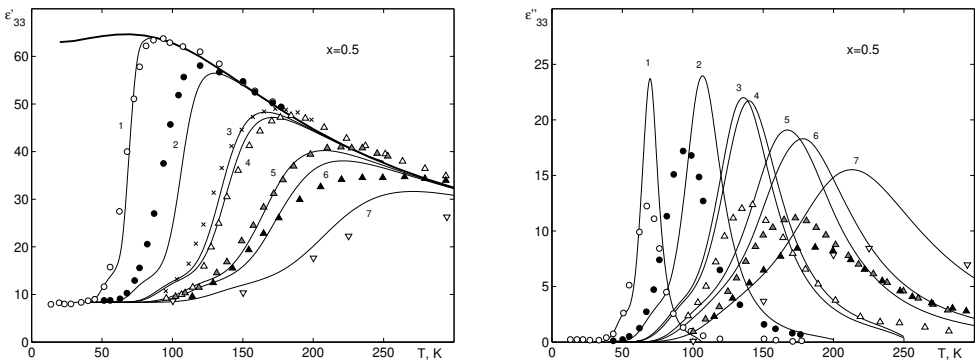

(a) (b)

Figure 8. The temperature dependences of real $\varepsilon'_{33}(T,\nu)$ (a) and imaginary $\varepsilon''_{33}(T,\nu)$ (b) parts of longitudinal permittivity for $Rb_{1-x}(ND_4)_xD_2PO_4$ at $x = 0.5$ and at different frequencies: 6 MHz – 1, 1' ○ [9]; 1 GHz – 2, 2', ● [9]; 8 GHz – 3, 3', × [10]; 10 GHz – 4, 4', △ [10]; 36 GHz – 5, 5', ▲ [10]; 52 GHz – 6, 6', ▲ [10]; 150 GHz – 7, 7', ▽ [10].

At low temperatures the experimental $\varepsilon'_{33}(T,\nu)$ rapidly decreases, because it is measured at non-zero frequencies. This decrease is qualitatively correctly described by the calculated real part of the dynamic permittivity $\varepsilon'_{33}(T,\nu)$ in the glass phase composition region, as shown in figure 8 for $Rb_{1-x}(ND_4)_xD_2PO_4$ at $x = 0.5$ and in figure 7 (dashed lines) for $Rb_{1-x}(NH_4)_xH_2AsO_4$ $x = 0.35$ (at ν=1 Hz, 30 kHz).

In the glass phase composition region the maximum of $\varepsilon''_{33}(T,\nu)$ (approximately coincides with the low-temperature inflection point of $\varepsilon'_{33}(T,\nu)$) corresponds to the temperature, at which the relaxation time is close to the field period. For $Rb_{1-x}(ND_4)_xD_2PO_4$ at $x = 0.5$ the calculated real and imaginary parts of $\varepsilon_{33}(T,\nu)$ at different frequencies satisfactorily describe the experimental data. The theory yields a faster decrease than the experiment for $\varepsilon'_{33}(T,\nu)$ and a narrower and higher peak for $\varepsilon''_{33}(T,\nu)$. We attribute this drawback to the imperfect procedure of configurational averaging of the susceptibility. In the case of $Rb_{1-x}(NH_4)_xH_2AsO_4$ the calculated imaginary part of $\varepsilon_{33}(T,\nu)$ has a very narrow and high peak. This discrepancy can be possibly caused by the

tunneling effects, essential in undeuterated compounds, which are not taken into account in our calculations performed within the Glauber dynamics approach.

At high temperatures the frequency dependence of the complex permittivity $\varepsilon(T,\nu)$ is close to the Debye type (figure 9). At low temperatures the Debye-type behavior disappears. In the

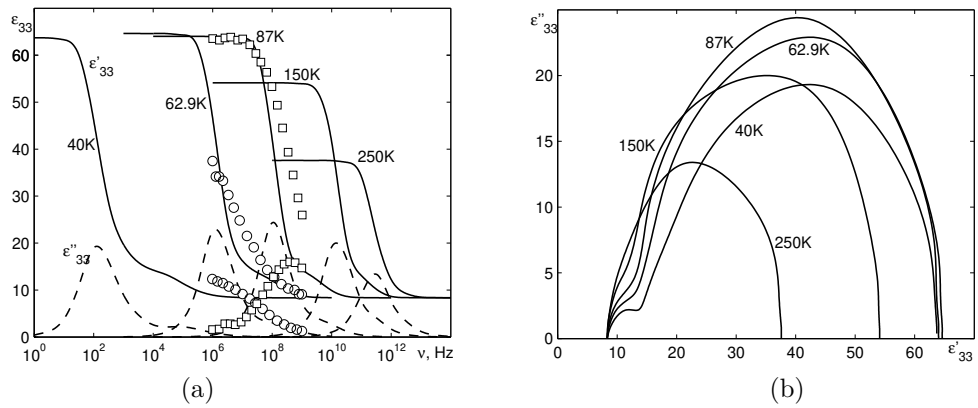

Figure 9. The frequency dependence of real $\varepsilon'_{33}(T,\nu)$ and imaginary $\varepsilon''_{33}(T,\nu)$ parts of longitudinal permittivity (a) for $Rb_{1-x}(ND_4)_xD_2PO_4$ at $x = 0.5$ at different temperatures: 40 K, 62.9 K ∘ [9], 87 K □ [9], 150 K, 250 K, and also the Cole-Cole curves (b) for these temperatures.

imaginary part of the permittivity a clear two-peak structure of the dielectric spectrum is observed. In the antiferroelectric phase the low-frequency peak is less pronounced.

We also calculated $\varepsilon'_{aa}(T,\nu)$, $\varepsilon''_{aa}(T,\nu)$ $(a = 1,3)$ in the regions of ferroelectric and antiferroelectric ordering. At low frequencies and at temperatures near and above $T_c(x)$ $\varepsilon'_{aa}(T,\nu)$ practically coincides with the static permittivity $\varepsilon_{aa}(T)$. At low temperatures $\varepsilon''_{33}(T,\nu)$ has a peak (correspondingly, $\varepsilon'_{33}(T,\nu)$ has a bend) (see figure 10 for $x = 0.2$).

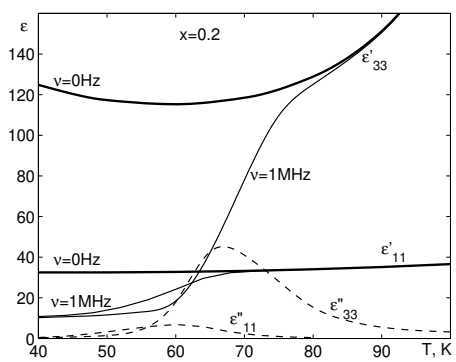

Figure 10. The temperature dependence of longitudinal $\varepsilon'_{11}(T,\nu)$ and transverse permittivities $\varepsilon'_{33}(T,\nu)$ for $Rb_{1-x}(ND_4)_xD_2PO_4$ compound for $x = 0.2$ at 1 MHz.

With lowering x the temperature position of this peak in $\varepsilon''_{aa}(T,\nu)$ practically does not change, but its height rapidly decreases. We failed to find this peak numerically at $x < 0.15$. A similar peak is detected in the antiferroelectric phase region at $0.65 < x < 0.70$. Let us note that for the same frequency $\varepsilon''_{11}(T,\nu) < \varepsilon''_{33}(T,\nu)$ for all concentrations x, what agrees with the experimental data.

It should be noted that both for the transverse and longitudinal permittivities the best description of experimental data is obtained in the regions of the so-called "pure" phases, that is $x \to 0$, $x \to 1$, and the glass phase region at $x \sim 0.5$ for $Rb_{1-x}(ND_4)_xD_2PO_4$ and $x \sim 0.35$ for $Rb_{1-x}(NH_4)_xH_2AsO_4$.

The proposed here approach can be used to describe of the dynamic characteristics of $Rb_{1-x}(ND_4)_xD_2PO_4$ compounds and to evaluate the qualitative behavior of the permittivities of $Rb_{1-x}(NH_4)_xH_2AsO_4$.

3.6. Phase diagrams

The phase diagrams of the $Rb_{1-x}(NH_4)_xH_2PO_4$ system are constructed, using the calculated physical characteristics of the crystals. The following regions are present in these diagrams: HP (high-temperature region of paraelectric phase), LP (low-temperature region of paraelectric phase), F (ferroelectric phase), AF (antiferroelectric phase) (figures 11, 12).

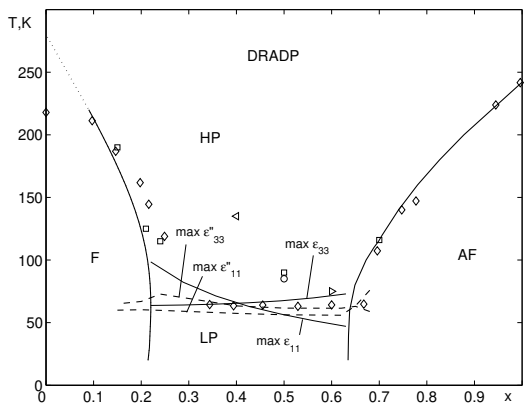

Figure 11. The phase diagram of the $Rb_{1-x}(ND_4)_xD_2PO_4$ mixture. ◁ – [7], ○ – [9], □ – [12], ▷ – [13], ◇ – [49]. The solid lines are the T_c, T_N, and T_g transitions obtained from the maxima of $\varepsilon_{33}(T)$ and $\varepsilon_{11}(T)$. The dashed lines are the T_g lines obtained from the maxima of $\varepsilon''_{33}(T,\nu)$ and $\varepsilon''_{11}(T,\nu)$ at frequency 1MHz.

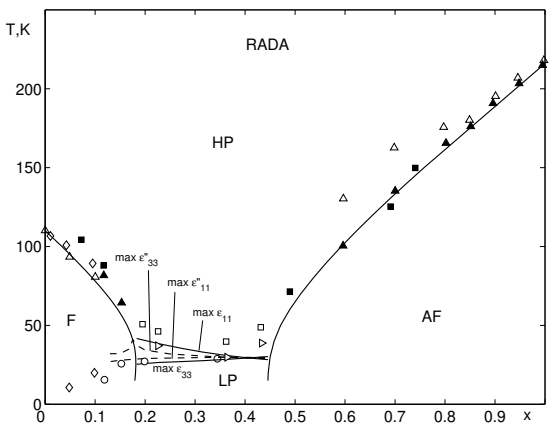

Figure 12. The phase diagram of the $Rb_{1-x}(NH_4)_xH_2AsO_4$ mixture. □ , ■ , ▷ – [17], ◇ – [18]; ○ – [94], △ , ▲ – [95]. The solid lines are the T_c, T_N, and T_g transitions obtained from the maxima of $\varepsilon_{33}(T)$ and $\varepsilon_{11}(T)$. The dashed lines are the T_g lines obtained from the maxima of $\varepsilon''_{33}(T,\nu)$ and $\varepsilon''_{11}(T,\nu)$ at frequency 30 kHz.

Typical peculiarities of the phase diagrams of the considered compounds will be discussed by the example of $Rb_{1-x}(ND_4)_xD_2PO_4$ (figure 11). At high temperatures the system is in paraelectric phase. It region is designated like the HP, because here the reduced Edwards-Anderson parameter Q_{EA} is small but different from zero and decreases with increasing temperature. For $x < 0.2$ and

$x > 0.65$ a spontaneous polarization or sublattice spontaneous polarization arise at $T < T_{\rm c}(x)$ and $T < T_{\rm N}(x)$, respectively. As a result, the system goes to the ferroelectric or antiferroelectric state. Here the reduced Edwards-Anderson parameter $Q_{\rm EA}$ can be significant (figure 5) in vicinities of $T_{\rm c}(x)$, $T_{\rm N}(x)$ and in ferroelectric phase for x close to glass phase composition region. In the central composition region we designate the low-temperature region of paraelectric phase. This region lies below the maxima of the static permittivities $\varepsilon_{11}(T)$ and $\varepsilon_{33}(T)$ (the solid lines in figures 11, 12) and attributes large value of $Q_{\rm EA}$. The dashed lines ($T_{g,11}(x,\nu)$ and $T_{g,33}(x,\nu)$) correspond to the low-temperature peaks of $\varepsilon''_{11}(T,\nu)$ and $\varepsilon''_{33}(T,\nu)$ at $\nu = 1$ MHz for $Rb_{1-x}(ND_4)_xD_2PO_4$ (the so-called freezing lines).These lines continue in the regions $x < 0.2$ and $x > 0.65$, where the paraelectric (or the proton glass) phase possibly coexists with ferroelectric or antiferroelectric phases, respectively. Numerical calculations show that $T_{g,11}(x,\nu) \to 0$ and $T_{g,33}(x,\nu) \to 0$ at $\nu \to 0$, so within the framework of our theory the averaged relaxation times for longitudinal and transverse permittivity have an Arrhenius-like temperature behavior that is $T_0 = 0$ (Vogel-Fulcher temperature). It should be noted that the approximation for the averaged relaxation times based on the experimental data ([10]) gives the value $T_0 \approx 32$ K for $x = 0.5$. The experimental points of [49] presented in this phase diagram were obtained by NMR studies.

The phase diagram of $Rb_{1-x}(NH_4)_xH_2AsO_4$ is strongly asymmetric (figure 12), and the proton glass composition region exists at $x = (0.2; 0.45)$. The freezing lines $T_{g,11}(x,\nu)$ and $T_{g,33}(x,\nu)$ (dashed lines) correspond to the maxima of $\varepsilon''_{11}(\nu = 30$ kHz,T) and $\varepsilon''_{33}(\nu = 30$ kHz,T). The approximation on the basis of experimental data ([17]) gives the value $T_0 \approx 30$ K for x=0.36. According to the experimental data [18, 94] $T_{g,11}(x,\nu)$ is observed in the ferroelectric phase down to $x = 0.01$. Also $T_{g,11}(x,\nu) \to 0$ with decreasing x. The calculations yield the freezing line down to $x \sim 0.15$. Overall, the calculated phase diagram correctly describes the available experimental lines, even though some discrepancies are present. Thus, at the accepted values of the theory parameters the glass phase composition region is somewhat wider $x \sim [0.18; 0.46]$ than the experimental one $x \sim [0.22; 0.42]$. This difference can be related with an incorrectly determined concentration x in experimental samples.

4. Conclusions

In the framework of the four-particle cluster approximation for the short-range interactions and the mean field approximation for the long-range interactions, we explored the free energy, a system of equations for variation parameters, expression for spontaneous polarization, Edwards-Anderson parameter, molar specific heat, longitudinal and transverse dielectric permittivities of the $Rb_{1-x}(ND_4)_xD_2PO_4$ and $Rb_{1-x}(NH_4)_xH_2AsO_4$ compounds for all compositions x. The theoretical results are compared with experimental data.

In the ferroelectric phase composition region, the spontaneous polarization decreases with increasing x and vanishes at the transition to the glass phase region. The molar specific heat of the $Rb_{1-x}(NH_4)_xH_2PO_4$ type compounds in the regions of the ferroelectric and antiferroelectric phases has jumps, which vanish at the transition to the proton glass phase composition region. The Edwards-Anderson parameter is different from zero at all compositions $0 < x < 1$ and temperatures, which is explained by the internal random deformational fields

For the $Rb_{1-x}(ND_4)_xD_2PO_4$ mixture the proposed theory satisfactorily describes the temperature curves of the real and imaginary parts of the longitudinal and transverse permittivities in the regions of "pure" phases ($x \sim 1$, 0.5, 0). At the same time, for $Rb_{1-x}(NH_4)_xH_2AsO_4$ at low temperatures in the glass phase composition region the theory incorrectly describes the shape of the imaginary part of the permittivity curves $\varepsilon''_{aa}(T,\nu)$ (the theoretical peak is too narrow and too high). This is partially caused by the neglected within the Glauber approach tunneling of protons, which plays an essential role in the dynamic processes in these systems at low temperatures. It is established that in this model the dynamics in the proton glass composition region is of the Debye relaxation type only at high temperatures. In our model the temperature curves of the averaged relaxation times for longitudinal and transverse permittivities for proton-glass composition region at $T \to 0$ are close to the Arrhenius law. The phase diagrams constructed using the calculated

dielectric characteristics are close to the experimental ones.

The absence of reliable experimental data for the physical characteristics of the $Rb_{1-x}(NH_4)_xH_2PO_4$ type proton glasses in a wide composition range poses huge difficulties in verifying the validity of the proposed theory. Possible further improvements of the theory of proton glasses also require reliable experimental data for the temperature dependences of all the calculated characteristics of these crystals in a wide composition range.

References

1. Courtens E., J. Phys. (Paris) Lett., 1982, **43** L199.
2. Nagata T., Iwata M., Orihara H., Ishibashi Y., Miura Y., Mamiya T., Terauchi H., J. Phys. Soc. Jpn., 1997, **66**, No. 5, 1503.
3. Takashige M., Terauchi H., Miura Y., Hoshino S., Nakamura T., Jap. J. Appl. Phys., 1985, **24** Suppl. 24–2, 947.
4. Iida S., Terauchi H., J. Phys. Soc. Jpn., 1983, **52**, 4044.
5. Courtens E., Phys. Rev. B, 1986, **33**, No. 4, 2975.
6. Samara G.A., Terauchi H., Phys. Rev. Lett., 1987, **59**, No. 3, 347.
7. Ko J.H., Kim B.G., Kim J.J., Fujimori H., Miyajima S., J. Phys.: Condens. Matter., 1995, **14**, 4403.
8. Miura Y., Takashige M., Terauchi H., Takano Y., Ishimoto H., Ogawa S., Jap. J. Appl. Phys., 1985, **24**, Suppl. 24–2, 950.
9. He P., J. Phys. Soc. Jpn., 1991, **60**, No. 1, 313.
10. Banys J., Kajokas A., Lapinskas S., Brillingas A., Grigas J., Petzelt J., Kamba S., J. Phys. B, 2002, **14**, 3725.
11. Courtens E., Vogt H., Z.Phys.B., 1986, **62**, 143.
12. Kutnjak Z., Pirc R., Levstik A., Levstik I., Filipic C., Blinc R., Phys.Rev., 1994, **50**, No. 17, 12421.
13. Levstik A., Filipic C., Kutnjak Z., Levstik I., Pirc R., Tadic B., Blinc R., Phys. Rev. Lett., 1991, **66**, No. 18, 2368.
14. Kim B.G., Kim J.J., Phys.Rev.B, 1997, **55**, No. 9, 5558.
15. Trybula Z., Schmidt V.H., Drumheller J.E., He D., Li Z., Phys. Rev.B, 1989, **40**, No. 7, 5289.
16. Trybula Z., Schmidt V.H., Drumheller J.E., Phys. Rev.B, 1991, **43**, No. 1, 1287.
17. Kim S., Kwun S., Phys. Rev. B, 1990, **42**, No. 1, 638.
18. Pinto J., Schmidt V.H., Ferroelectrics, 1993, **141**, 207.
19. Gridnev S.A., Korotkov L.N., Shuvalov L.A., Rogova S.P., Fedosyuk R.M., Ferroelectrics Lett., 1991, **13**, 67.
20. Gridnev S.A., Sorosovskii obozrevatelnyi zhurnal, 1998, No. 8, 95 (in Russian).
21. Tu C.S., Schmidt V.H., Saleh A.A., Phys. Rev. B., 1993, **48**, No. 17, 12483.
22. Ono Y., Hikita T., Ikeda T., J. Phys. Soc. Jpn., 1987, **56**, No. 2, 577.
23. Kwon O.J., Kim J.J., Phys.Rev B, 1993, **48**, No. 9, 6639.
24. Cevc P., Zalar B., and Blinc R., Solid state Comm., 1989, **70**, No 4, 461.
25. Kind R., Blinc R., Dolinsek J., Korner N., Zalar B., Cevc P., Dalal N., DeLooze J., Phys. Rev. B, 1991, **43**, No. 4, 2511.
26. Grinberg E.S., Izotov V.V., Efimov V.N., Ferroelectrics Letters, 1993, **15**, 61.
27. Smolyaninov I., Glinchuk M.D., J.Phys.: Condens.Matter, 1994, **6**, 2869.
28. Slak J., Kind R., Blinc R., Courtens E., Zumer S., Phys. Rev. B, 1984, **30**, No. 1, 85.
29. Chen S., Ailion D.C., Laicher G., Phys. Rev. B, 1993, **47**, No.6, 3047.
30. Terauchi H., Ferroelectrics, 1985, **64**, 87.
31. Cowley R.A., Ryan T., Courtens E., J. Phys. C: Solid State Phys., 1985, **18**, 2793.
32. Hayase S., Sakashita H., Terauchi H., Ferroelectrics, 1987, **72**, 245.
33. Yuzyuk Yu.I., Gregora I., Vorlicek V., Pokorny J., Petzelt J., J. Phys.: Condens. Matter, 1995, **7**, 683.
34. Yuzyuk Yu.I., Gregora I., Vorlicek V., Petzelt J., J. Phys.: Condens. Matter, 1996, **8**, 619.
35. Hattori T., Araki H., Nakashima S., Mitsuishi A., Terauchi H., J. Phys. Soc. Jpn., 1988, **57**, No. 3, 1127.
36. Popkov Yu.A., Vankevich A.V., Shuvalov L.A., Fedosyuk R.M., Fizika nizkih temperatur, 1993, **19**, No. 2, 195 (in Russian).
37. Kim J.J., Shin H.K., Ferroelectrics, 1992, **135**, 319.
38. Blinc R., Dolinsek J., Schmidt V.H., Ailion D.C., Europhys. Lett., 1988, **6**, No. 1, 55.
39. Chen S., Ailion D.C., Phys.Rev.B, 1990, **42**, No. 10, 5945.

40. Seliger J., Zagar V., Blinc R., Phys. Rev. B, 1995, **52**, No. 17, 12519.
41. Grimm H., Parlinski K., Schweika W., Courtens E., Arend H., Phys. Rev. B, 1986, **33**, No.7, 4969.
42. Choi Y.S., Kim J.J., Eur.Lett., 2004, **65**, No. 1, 55.
43. Chamberlin R.V. and Haines D.N., Phys.Rev.Lett., 1990, **65**, N 17, 2197.
44. Chamberlin R.V., Phys. Rev. B, 1993, **48**, No. 21, 15638.
45. Blinc R., Dolinsek J., Zalar B., Z. Phys. B, 1997, **104**, 629.
46. Sinitskii A., Schmidt V.H., Phys. Rev. B, 1996, **54**, No.2, 842.
47. Moriya K., Matsuo T., Suga H., Terauchi H., Jap. J. Appl. Phys., 1985, – 24 Suppl. 24-2, 955.
48. Papantopoulos G., Papavassiliou G., Milia F., Schmidt V.H., Drumheller J.E., Pinto N.J., Blinc R. Zalar B., Phys. Rev. Lett., 1994, **73**, No. 2, 276.
49. Korner N., Pfammatter Ch., Kind R., Phys. Rev. Lett., 1993, **70**, No. 9, 1283.
50. Noh K.H., Kwun S., Yoon J.G., Phys. Rev. B, 2000, **62**, 223.
51. Trybula Z. Kaszynski J., Ferroelectrics, 2004, **298**, 347.
52. Eom J., Yoon J., Kwun S., Phys. Rev. B, 1991, **44**, No.6, 2826.
53. Trybula Z. and Kaszynski J., Maluszynska H., Ferroelectrics, 2005, **316**, 125.
54. Korotkov L.N., Shuvalov L.A., Ferroelectrics, 2003, **285**, 67.
55. Kaszynski J., Trybula Z., Maluszynska H., Acta Physica Polonica A, 2005, **108**, No. 1, 103-106.
56. Lanceros-Mendez S., Schmidt V.H., and Shapiro S.A., Ferroelectrics, 1999, **223**, 203.
57. Howell F.L., Pinto N.J., Schmidt V.H. Phys. Rev. B, 1992, **16**, No. 21, 13762.
58. Trybula Z. and Kaszynski J., Los Sz., Mielcarek S., and Trybula M., Phys. Stat. Sol. (b), 2004, 241, No. 2, 447.
59. Gregorovic A., Zalar B., Blinc R., Ailion D.C., Phys.Rev.B, 1999, **60**, No. 1, 76.
60. Schmidt V.H., Lanceros-Menndez S., Meschia S.C., Pinto N.J., Solid State Ionics, 1999, **125**, 147.
61. Tu C.S., Schmidt V.H., Ferroelectrics, 1999, **227**, 141.
62. Schmidt V.H., J.Korean Phys.Soc., 1998, **32**, S803.
63. Dobrosavljevic V., Stratt R.M., Phys. Rev. B, 1987, **36**, No.16, 8484.
64. Tadic B., Pirc R., Blinc R., Phys. Rev. B, 1988, **37**, No.1, 679.
65. Sherrington D., Kirkpatrick S., Phys. Rev. Lett., 1975, **35**, 1792.
66. Pirc R., Tadic B., Blinc R., Phys. Rev. B, 1987, **36**, No. 16, 8607.
67. Kim D.H., Kim J.J., Ferroelectrics, 2002, **268**, 263.
68. Blinc R., Dolinsek J., Pirc R., Tadic B., Zalar B., Kind R., Liechti O., Phys. Rev. Lett., 1989, **63**, No. 20, 2248.
69. Pirc R., Tadic B., Blinc R., Kind R., Phys. Rev. B, 1991, **43**, No. 4, 2501.
70. Crokidakis N., Nobre F.D., Phys. Rev. E, 2008, **77**, 041124.
71. Banerjee V., Dattagupta S., Phys. Rev B, 2003, **68**, 054202.
72. Prelovcek P., Blinc R., J. Phys. C.: Solid State Phys., 1982, **15**, L985.
73. Matsushita E., Matsubara T., Prog.Theor.Phys., 1984, **71**, No. 2, 235.
74. Matsushita E., Matsubara T., J. Phys. Soc. Jap., 1985, **54**, No. 3, 1161.
75. Korynevskii N.A., Solovyan V.B., Ferroelectrics, 2005, **317**, 19.
76. Korynevskii N.A., Solovyan V.B., Phase Transition, 2007, **80**, No. 1-2, 55.
77. Korynevskii N.A., Solovyan V.B., Condens. Matter Phys., 2009, **12**, No 2, 267.
78. Levitskii R.R., Sorokov S.I., Vdovych A.S., Ferroelectrics, 2005, **316**, 111.
79. Sorokov S.I., Levitskii R.R., Vdovych A.S., Condens. Matter Phys., 2005, **8**, No. 3(43), 603.
80. Sorokov S.I., Vdovych A.S., Levitskii R.R., J. Phys. Study, 2009, **13**, No. 1, 1701 (in Ukrainian).
81. Sorokov S.I., Vdovych A.S., Levitskii R.R., Preprint of the Institute for Condensed Matter Physics, ICMP-09-06U, Lviv, 2009 (in Ukrainian).
82. R.R. Levitskii, S.I. Sorokov, J. Stankowski, Z. Trybula, A.S. Vdovych, Condens. Matter Phys., 2008, **11**, No. 3(55), 523.
83. Sorokov S.I., Levitskii R.R., Vdovych A.S., Ferroelectrics, 2009, **379**, Issue 1, 101.
84. Stasyuk I.V., Levitskii R.R., Phys. Stat. Sol. b, 1970, **39**, No. 1, K35.
85. Levitskii R.R., Zachek I.R., Vdovych A.S., Sorokov S.I., Condens. Matter Phys., 2009, **12**, No 1, 75.
86. Fairall C.W., Reese W., Phys. Rev. B, 1974, **10**, No. 3, 882.
87. Zolototrubov Yu.S., Strukov B.A., Taraskin S.A., Kamisheva L.N., Izv. AN SSSR, ser. fiz., 1975, **39**, No. 4, 782 (in Russian).
88. Amin M., Strukov B.A., Fiz. Tverd. Tela, 1970, **12**, No. 7, 2035 (in Russian).
89. Stephenson C.C., Adams H.E., J. Am. Chem. Soc., 1944, **66**, No. 8, 1409.
90. Mason W.P., Mattias B.T., Phys. Rev., 1952, **88**, No. 3, 477.
91. Vasilevskaya A.S., Sonin A.S., Fiz. Tverd. Tela, 1971, **13**, No. 6, 1550 (in Russian).

92. Blinc R., Burgar M., Levstik A., Sol. Stat. Commun., 1973, **12**, No. 6, 573.
93. Berdowski J., Opilski A., J. Crystal Growth, 1978, **43**, 381.
94. Trybula Z, Stankowski J., Condens. Matter Phys., 1998, **1**, No. 3(15), 311.
95. Trybula Z, Stankowski J, Szczepanska L., Blinc R., Weiss Al., Dalal N.S., Ferroelectrics, 1988, **79**, 335.

Термодинаміка, діелектрична проникність і фазові діаграми протонних стекол типу $Rb_{1-x}(NH_4)_xH_2PO_4$

С.І. Сороков, Р.Р. Левицький, А.С. Вдович

Інститут фізики конденсованих систем НАН України, 79011 Львів, вул. Свєнціцького, 1

Кластерна псевдоспінова модель протонних стекол, яка враховує енергетичні рівні протонів біля тетраедрів PO_4, далекосяжну взаємодію між водневими зв'язками і внутрішнє хаотичне деформаційне поле застосовується для дослідження термодинамічних характеристик та поздовжньої і поперечної діелектричних проникностей $Rb_{1-x}(ND_4)_xD_2PO_4$ та $Rb_{1-x}(NH_4)_xH_2AsO_4$ сполук. Виконано огляд експериментальних і теоретичних робіт присвячених кристалам типу $Rb_{1-x}(NH_4)_xH_2PO_4$.

Ключові слова: *протонне скло, діелектрична проникність*